CONSTRAINTS ON THE PETROGENESIS OF A PROTEROZOIC TALC DEPOSIT IN SOUTHWESTERN MONTANA: A PETROLOGICAL AND GEOCHEMICAL STUDY

by

Monica Marie McGrath

B.S. Geology, Juniata College, 2013

Submitted to the Graduate Faculty of the

Kenneth P. Dietrich School of Arts and Sciences in partial fulfillment

of the requirements for the degree of

Master of Science in Geology

University of Pittsburgh

2017

UNIVERSITY OF PITTSBURGH

Kenneth P. Detrich School of Arts and Sciences

This thesis was presented

by

Monica M. McGrath

It was defended on

August 8th, 2017

and approved by

Dr. Joesf Werne, Professor, Director of Graduate Studies, Geology and Environmental Science

Dr. Rosemary Capo, Associate Professor, Geology and Environmental Science

Thesis Director: Dr. Brian Stewart, Associate Professor, Geology and Environmental Science

CONSTRAINTS ON THE PETROGENESIS OF A PROTEROZOIC TALC DEPOSIT IN SOUTHWESTERN MONTANA: A PETROLOGICAL AND GEOCHEMICAL STUDY

Monica M. McGrath, M.S.

University of Pittsburgh, 2017

Talc, a magnesium phyllosilicate, is used in many products, including paints, rubber, ceramics, cosmetics and plastics. Talc mineralization generally occurs in low-grade metamorphic conditions and requires a significant source of magnesium. Large amounts of Al, Ca, or K in the formational environment limit talc mineralization in favor of other minerals such as chlorite, tremolite and biotite. Formation processes, such as metamorphism or hydrothermal events, of the talc bodies control the inherent compositions and can dictate which impurities are present. This study focuses on a talc deposit near Alder, Montana, one of a series of high purity Precambrian deposits within this region. Petrographic results indicate that dolomitic marble was pseudomorphically replaced by talc. This implies that sufficient magnesium was supplied from the host rock and silica was supplied by the hydrothermal fluid. Relatively pure (>90% by XRD) talc samples have only trace amounts of Al, Ca, and K, and are very low in rare earth elements (REE), with generally flat chondrite-normalized REE patterns. For these samples, the most common accessory mineral is clinochlore. Acetic acid leachates from carbonate-rich units yield light REE enriched patterns and higher REE concentrations than the pure talc samples. Rare earth element patterns and concentrations suggest that the talc inherited its REEs from the carbonate during recrystallization from carbonate to talc. Sm-Nd isotope data from the carbonate samples define a linear trend corresponding to an age of 1.42±0.07 Ga, which is consistent with the inferred age of the hydrothermal event responsible for the talc formation.

TABLE OF CONTENTS

LIST OF TABLES

LIST OF FIGURES

ACKNOWLEDGEMENTS

Thank you to RJ Lee Group for provided funding and samples for this project. Additional, thank you for providing resources and analytical tools to complete many aspects of this project.

I would like to acknowledge and extend my gratitude to my colleagues Bryan Bandli and Monica Carse for providing guidance and support throughout this process. Matt Sanchez thank you taking me under you wing, becoming a mentor, and providing me this opportunity. I am beyond grateful. Lastly, thank you to my advisor Brian Stewart for taking on this project and providing the tools, knowledge, and expertise to approach this problem in a new way.

Justin Koerner, thank you for being my rock, for standing by me and supporting be during all my academic years.

To my mom and sister, thank you for the continual unconditional love and support.

This thesis is dedicated to my father

John F. McGrath

“Forever grateful to boldly go there

and back again.”

1.0 INTRODUCTION

1.1 PROPERTIES AND USES OF TALC

Talc, $Mg_3Si_4O_{10}(OH)_2$, is a versatile phyllosilicate mineral with applications in industry agriculture, and consumer products, including but not limited to the manufacturing of paper, paints, plastics, rubber, cosmetics, and pharmaceuticals. Talc can form in either a compact or platy microcrystalline form, often as soapstone, a soft metamorphic rock composed primarily of talc with a massive or schistose texture (Klein and Dutrow, 2008). Talc has a trioctahedral "T-O-T" structure with perfect cleavage on [001]. Talc has very little variation in chemical composition; small amounts of Al or Ti may substitute for Si and Fe may replace Mg. Talc is commonly associated with other silicate minerals such as amphibole, serpentine and chlorite, which are also magnesium silicates found mineralizing in similar environments as talc. If these minerals are present within the talc ore, they could cause contamination of products produced from the talc and affect the grade of talc. Talc is separated into three different grades; from lowest to highest, these are industrial grade, food grade, and cosmetic grade. Ultimately the talc grade is driven by the end-users' requirements which include color or whiteness, particle size, mineralogy, absence of asbestos, and potentially any physical priority requirements for end use.

1.2 TYPES OF TALC DEPOSITS

Talc commonly occurs in fault zones that cut mafic, ultramafic, and/or metamorphic rocks (Kesler, 1994). The temperature stability field for talc ranges from 100°C to 700°C depending on the pressure. It mineralizes as a function of the availability of Mg during low-grade metamorphic or hydrothermal events. Talc can form by alteration of magnesium silicate minerals such as olivine, pyroxene and amphiboles, and is often found as a pseudomorph of these minerals. The mineralogy of any given talc deposit is controlled by the nature of the protolith, fluid composition, and the temperature and pressure range during formation. Large amounts of Al, Ca, or K in the formational environment limit talc mineralization in favor of other minerals such as chlorite, tremolite and biotite (Greenwood, 1998). The compositions of the rock units hosting talc often dictate which impurities are present within the talc.

Talc generally mineralizes by one of four processes (McCarthy (2015)): (1) alteration of serpentinite (i.e., ultramafic origin talc); (2) hydration of mafic rock to serpentine, followed by subsequent alteration to talc-carbonate (i.e., mafic origin talc); (3) hydrothermal alteration of dolomitic host by silica-rich fluid (i.e., metasedimentary origin talc); and (4) alteration of siliceous dolostones to tremolite/actinolite followed by partial conversion to talc by metamorphism (i.e., metamorphic origin talc). The metasomatism of talc causes interaction that removes chemical components of the host rock and introduces new components through the fluids. This results in fewer mineral phases than during a dry metamorphic event due to the removal of key chemical components.

1.3 OBJECTIVE OF THESIS

This project aims to investigate and further constrain the geologic processes that result in large body talc deposits through investigation of a talc unit in the talc mining district of southwest Montana. The purpose of this investigation is to explore the relationships of the talc with the surrounding rock bodies using strontium and neodymium isotope systems, along with other petrological and geochemical data gathered from thin section petrography, XRD, XRF and ICP-MS. These data allow us to form a more complete history of how the talc mineralized within this region, and to constrain about the fluids that would have been present in the system as well as the minerals that would have precipitated from these conditions.

The importance of this study and others like it stems from debate over the past 40 years of the potential health effects of talc and its potential to be associated with hazardous asbestos minerals. Talc can occur in close proximity or cogenetically with asbestos minerals such as chrysotile, tremolite, actinolite, and anthophyllite due to similarity of mineralization environments and compositions. However, talc formed by certain processes, such as hydrothermal alteration of dolomite (process (3) above), is much more likely to be free of impurities than talc formed via intermediated silicate minerals (e.g., processes (1) and (4), above). Thus, it is critical not only to characterize but to understand the petrogenesis of potential ore grade talc deposits.

2.0 GEOLOGIC SETTING

2.1 HISTORY OF MONTANA TALC INDUSTRY

The talc deposits in Southwestern Montana contain some of the highest purity talc observed in the world. The region has three actively producing mines, along with many historic and prospective mines (Gunter et al., 2016). Whiter, purer talc is derived largely from dolomitic marbles rather than from ultramafic or mafic host rocks, because the former have fewer components, especially Al and Si, that can form other minerals within the talc. The talc from Montana is a high enough quality to meet all USP and CTFA requirements for cosmetic grade talc and usually does not require benefaction, thus reducing processing cost (Gunter et al., 2016). The three actively producing mines in Montana lie within a region referred to as the "talc corridor" (Childs, 2016), and comprise the Yellowstone Mine located in the Gravelly Range, as well as the Regal and Treasure Mines located in the Ruby Range (**Figure 1)**. Each of these mines has reserves of high purity talc in the millions of tonnes range and should continue to produce for decades to come (Cerino et al., 2007). The three actively producing mines have approximately ~18 million tonnes of talc reserves as of Dec. 2014 (Childs, 2016). In 2014, Montana was the leading supplier of talc within the USA, producing ~400KT out of a total of ~550 KT from the USA (McCarthy, 2016). These mines were the first sources of soapstone talc mined within the United States (Grexa and Parmentier, 1979). Besides the three active mines,

there are several historic mine and prospects within the talc corridor that have produced many tons of talc in the past or are predicted to produce well into the future.

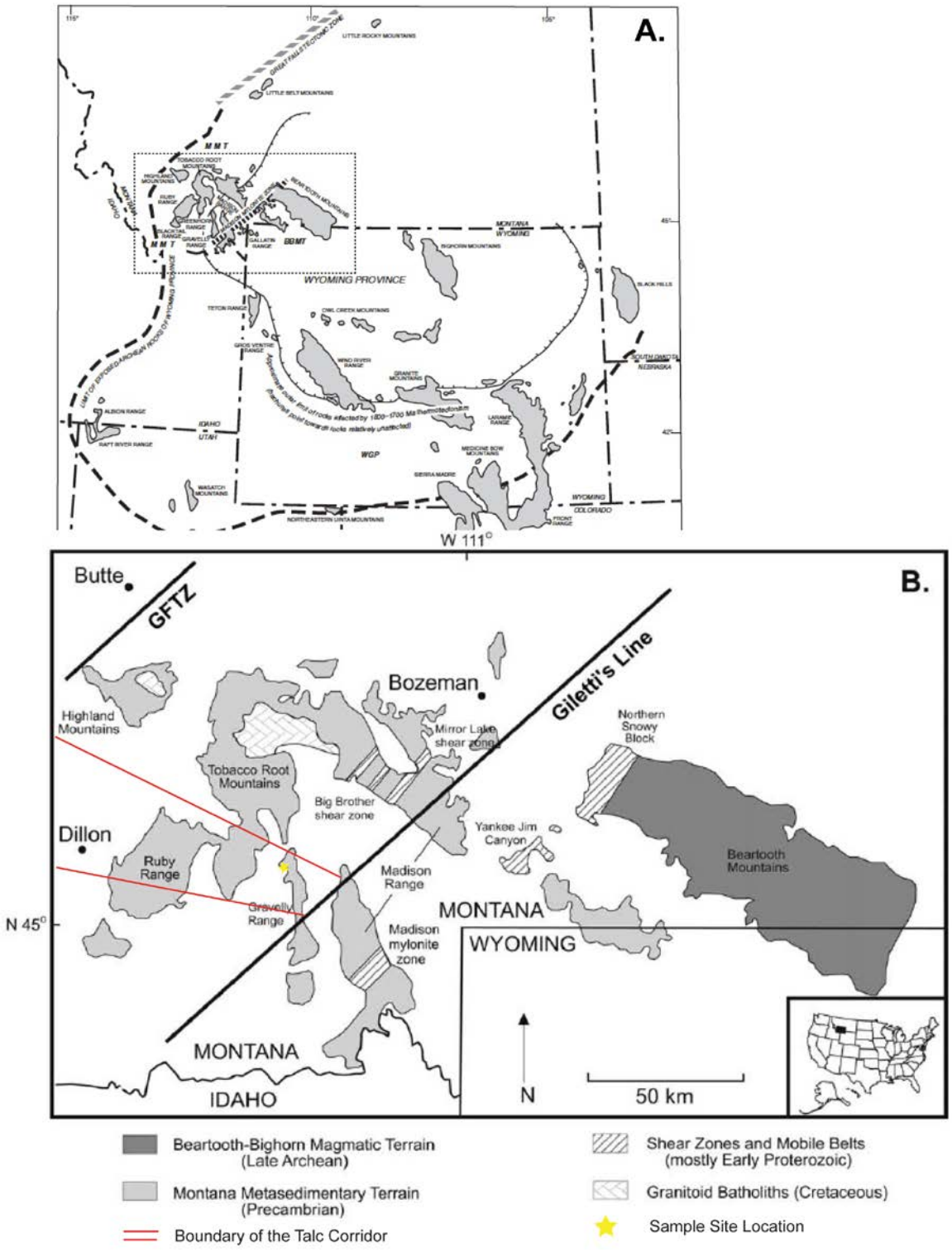

Figure 1: A) Geologic map of major terranes in the Wyoming Province. B) Geologic map of major mountain ranges with MMT and the Talc Corridor. (Modified from Roberts et al. 2002; Burger et al. 2004; Childs 2016 and references within).

2.2 GEOLOGY OF SOUTHWESTERN MONTANA

The Montana talc corridor is located within the Wyoming Province, a region in northwestern Wyoming and southwestern Montana consisting of approximately 100,000 km^2 of middle Archean craton (**Figure 1, 2**). The Wyoming province is split into three sub-provinces known as the Beartooth-Bighorn magmatic zone (BBMZ), the Montana metasedimentary terrane (MMT), and the Wyoming greenstone terrane (WGT) (Childs, 2016). Talc deposits located within the MMT are associated with dolomitic marble (Cerino et al., 2007).

Within the MMT, dolomitic marbles are associated with minor calcite, chlorite, phlogopite and graphite (Brady, 2004; Cheney et al., 2004). Some calcite marbles with accessory minerals such as phlogopite, dolomite, forsterite, tremolite and apatite can also be found within the area (Berg, 1979). These calcitic marbles appear to be at a higher metamorphic grade than the dolomitic marbles with very little to no alteration and are not directly associated with the talc (Berg, 1979). Unaltered dolomitic non-talc marble is also seen in the MMT. These marbles, along with the talc deposits, are a part of the Cherry Creek metamorphic suite (Mann, 1960). The MMT contains isoclinal folds and metamorphosed ortho-quartzites with marbles, pelitic schist, granulite and quartzofeldspathic gneisses. In the MMT, the metasedimentary rock package shows ε_{Nd} consistent with intercratonic or cratonic margin setting (Frost et al., 2003), indicating that these rocks were deposited in either one large basin or several smaller basins at ~2.65 Ga. This supracrustal sequence appears to have been part of one or many back-arc basin(s) formed on or near the Wyoming Archean craton.

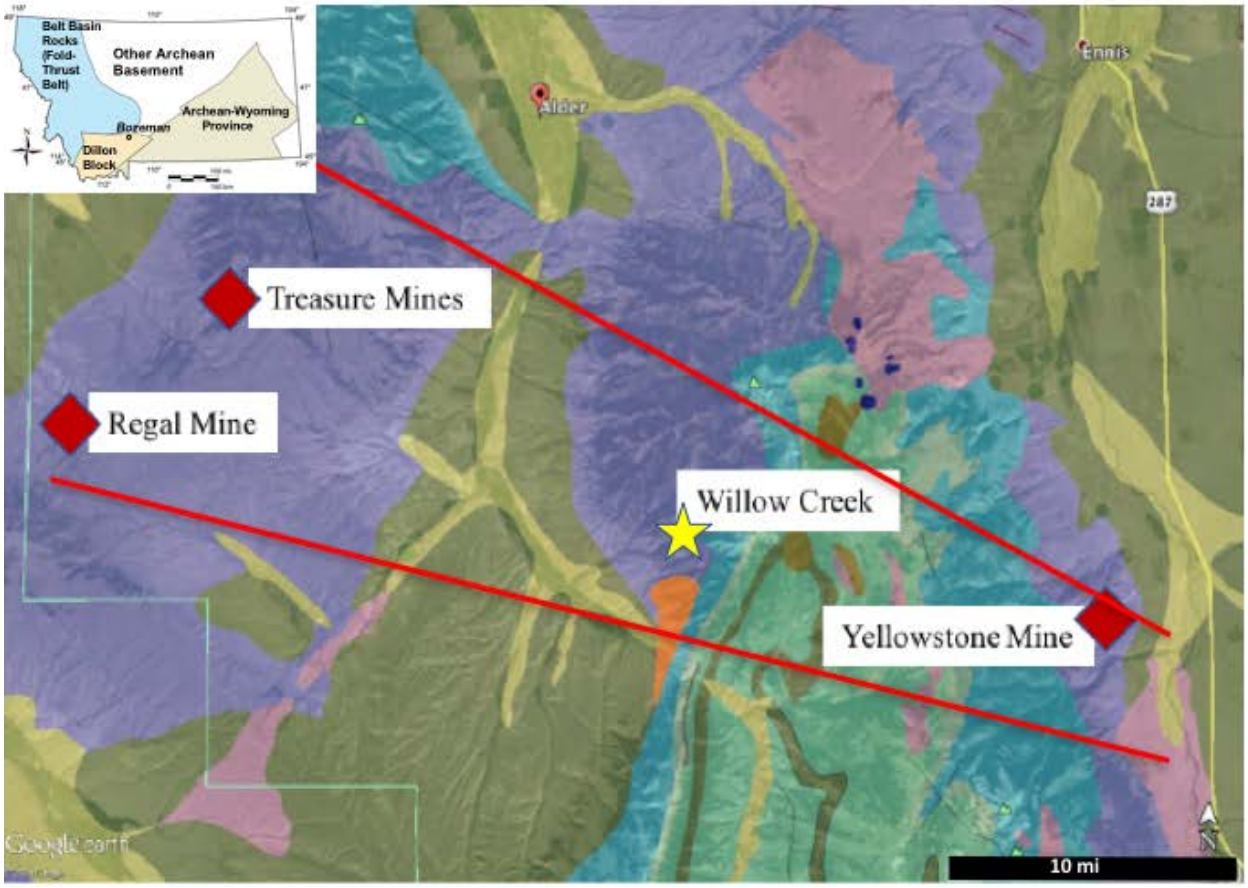

Figure 2: Geologic map of sample area including site location indicated by star. Red lines define area of talc corridor (Childs 2016). Purple - Metasedimentary marbles, gneiss, and talc schist. Orange - Boulder Batholith. Others - Phanerozoic sedimentary rocks.

2.3 TIMING OF EVENTS IN MMT

The Wyoming province has a complex tectonic and metamorphic history. Studies of metamorphic and detrital zircons have provided approximate dates for different tectonic and metamorphic events, including dates from U-Pb and Lu-Hf isotopic systems (summarized in **Figure 3**). The earliest detrital zircon dates from within the province suggest that deposition of sediments, specifically quartzite, was between 2.75 and 3.2 Ga, based on

a regional study conformably interbedded thin quartzites and paragneiss (Mueller et al., 1998; Childs, 2016). Mueller and Cordua (1976) proposed the 2.7-3.2 Ga date based on a Rb-Sr isochron reported by James and Hedge (1980) and lack of zircons younger than 2.8 Ga. This date indicates the sediments would have to be deposited prior to the first metamorphic event at 2.75 Ga. The youngest detrital zircons indicate a maximum deposition age rather than a minimum depositional age (Roberts et al., 2002). A reinterpretation by Roberts et al. (2002) indicates that there is no isotopic evidence to support the MMT deposition before 2.8 Ga, and they suggest that the 2.75 Ga event would have reset the Rb-Sr isochron reported by James and Hedge (1980) Roberts et al. (2002) suggest that the rocks within the MMT were deposited onto Middle Archean basement gneisses during the Late Archean to Early Proterozoic. This interpretation is supported by ^{40}Ar-^{39}Ar and ^{207}Pb-^{206}Pb ages of metamorphism obtained from biotite, amphiboles and garnets within the MMT reported by Roberts et al. (2002) and Brady et al. (2004).

The first metamorphism (M1) is inferred to have occurred between 2.7 and 2.4 Ga. M1 was upper amphibolite to granulite grade, as indicated by a calcite-olivine-phlogopite ± tremolite assemblage (Anderson et al., 1990). Temperatures during M1 reached 645-745°C, but possibly as high as 700-800°C at ~0.2 GPa (Alcock et al., 2013; Anderson et al., 1990; Gerwin, 2006). During this time rocks experienced 2-4 generations of folding, which is still preserved in the talc-bearing marble units (Anderson et al., 1990). A second metamorphism (M2) took place at 1.82-1.81 Ga and 1.78 and 1.74 Ga. A $\delta^{18}O$ study by Karasevich (1980) suggests that granitic intrusions were associated with the ~1.8 Ga event (M2) in the Tobacco Root Range. Monazite U-Th-Pb ages from the southern Ruby Range indicate prograde metamorphism at 1.83-1.81 Ga, and 1.78 Ga intrusion of an ultramafic magma (Alcock et al., 2013).

Subsequently, the area experienced emplacement of mafic dikes near 1.425 Ga, which led to a localized hydrothermal event. This event is thought to be responsible for much of the talc formation (Anderson et al., 1990; Brady et al., 1998). Both the Ruby and Tobacco Root Ranges are North and West of the Willow Creek deposit, inferring that these intrusions would have supplied the heat that mineralized the talc. These intrusion may have also caused the faulting and sheering that acted as conduits for the fluid that allowed talc to mineralize. The area remained relatively dormant except for deposition of Phanerozoic sediments and major uplift associated with Late Cretaceous Laramide orogeny caused major uplift (Burger, 2004).

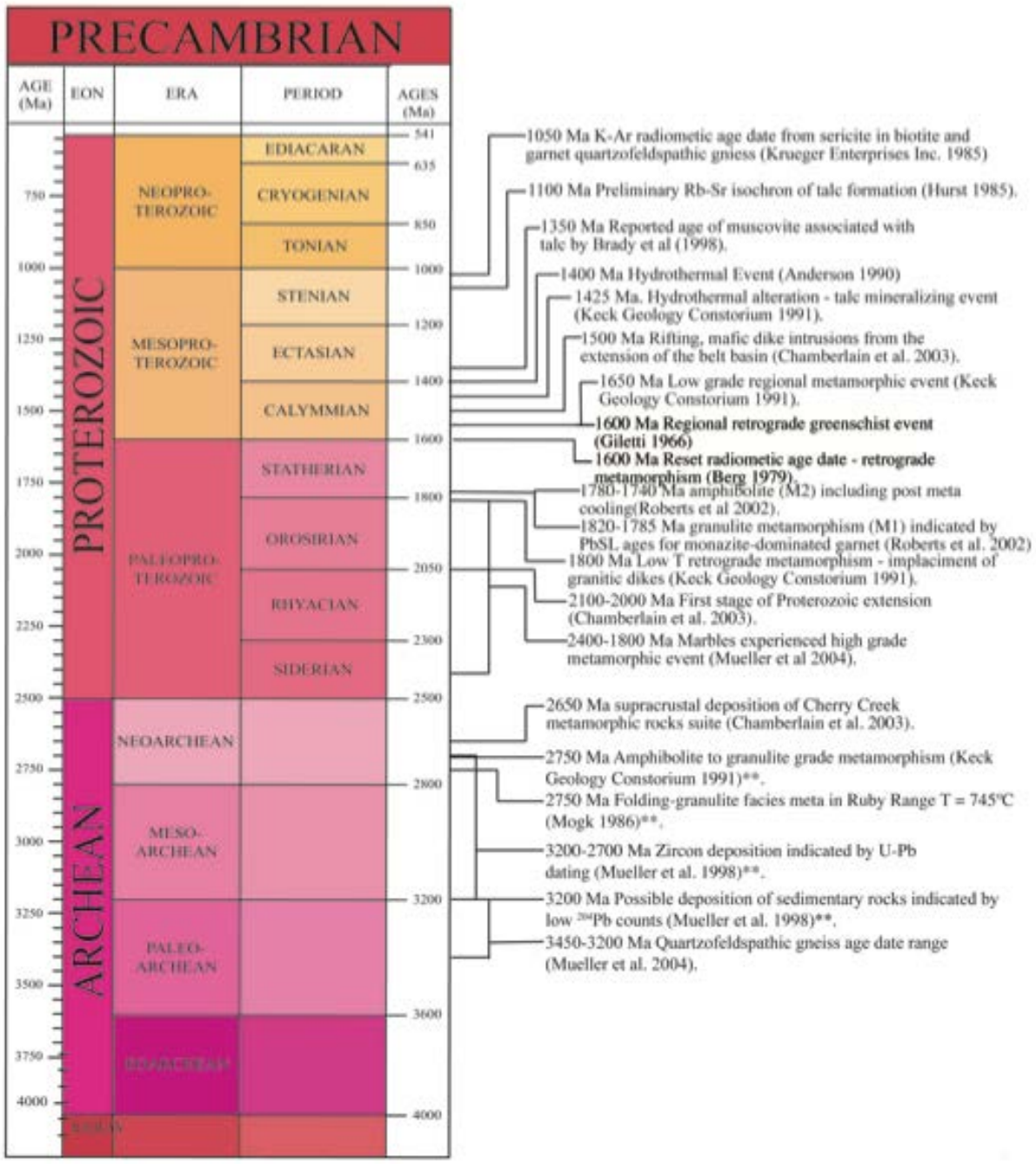

Figure 3: Sequence of talc mineralization and other events in the MMT. Geologic timescale from Walker et al. (2012).

2.4 TECTONIC HISTORY OF MMT

The Wyoming province experienced two pulses of Proterozoic extension at ~1.8-2.0 Ga and ~1.4-1.5 Ga. This second period of extension had much more of an effect on southwestern Montana than the first period of extension, which affected the eastern half of the Wyoming province. Near 1.5 Ga, rifting started in relation to the opening of the Belt basin to the northwest of the MMT. Some authors use the term 'Pre-Belt' to define the mafic and metamorphic rocks that form the crystalline basement for the middle Proterozoic Belt basin in the Dillion Tectonic Block of southwestern Montana which includes both Archean and Paleoproterozoic rocks (Childs, 2016). These 'Pre-belt' rocks consist of the calcite- and dolomite-rich marbles that were replaced in a volume by volume replacement with talc. The Proterozoic rifting allowed for the intrusion of mafic dike in parts of the MMT, in theory providing the heat for the system. N-S striking normal faults are present surrounding and passing through the ore bodies of the Yellowstone mine which provided the "plumbing" or fluid conduits for the talc mineralization (Cerino et al., 2007). Other faults with the same strike contain chlorite and possibly predate the talc formation (Cerino et al., 2007).

Laramide uplifts within the Wyoming province are widely spread and discontinuous. In the MMT the uplifted blocks have a northwest-southeast trend and are bounded by reverse faulting. Frost et al. (2003) proposed that the Laramide orogeny reactivated the Archean basement structures. This suggests that either these Archean structures are more pronounced and weaker than those developed later during the Belt basin extension or that the Laramide created localized stress fields within the Wyoming province that were nearly parallel to already existing structures.

2.5 WILLOW CREEK DEPOSIT

This study focuses on the Willow Creek deposit within the Dillion block in SW Montana (**Figure 2**). This region outside of Alder was extensively studied by Berg (1979). Mining ceased in 1979 and the mine was closed. At this site, Archean age marbles and hydrothermally altered talc ore is present. The dominant lithology throughout the region of the Dillion block is a quartzofeldspathic gneiss (the Dillion Gneiss). Currently, two individual metamorphic events and a later hydrothermal event have been described and documented (Alcock et al., 2013; Anderson et al., 1990; Berg, 1979; Gammons and Matt, 2002; Roberts et al., 2002). The main talc forming event was this later hydrothermal alteration (M3) of the dolomitic marble to talc (Anderson et al., 1990). The large volumes of fluids needed for these reactions was most likely provided by connate brine waters pushed up from old sedimentary basin as the Belt Basin opened during the Laramide (Gammons and Matt, 2002). Another possible fluid source was Proterozoic seawater, although preliminary fluid inclusion data suggest that the NaCl content in the inclusions was too high to be sea water (Gammons and Matt, 2002).

3.0 METHODS

3.1 SAMPLE COLLECTION AND INITIAL EVALUATION

Thirteen samples were collected from the field site by M. Sanchez (RJ Lee Group), encompassing both the unaltered marble zone and the main talc zone (**Fig. 4)**. Weathering and slump have reclaimed portions of the mine and the lower benches are no longer visible (**Figs. 5, 6**). Seven samples were collected from main talc zone, two from the unaltered marble zone, one from the chloritic alteration zone, and one from outside the mine pit (**Table 1)**. Samples were collected to represent the talc-containing rocks and were not always collected in place. Preliminary mineral identification was made using grain mounts in refractive index liquids. Suspect minerals were picked out and examined in R.I. liquids 1.400 – 1.700. These grain mounts help determine where thin sections were going to be made. Double polished thick (200 microns) and thin (30 microns) sections were made at Vancouver Petrographics LTD. Samples were examined using Leica petrographic microscopes.

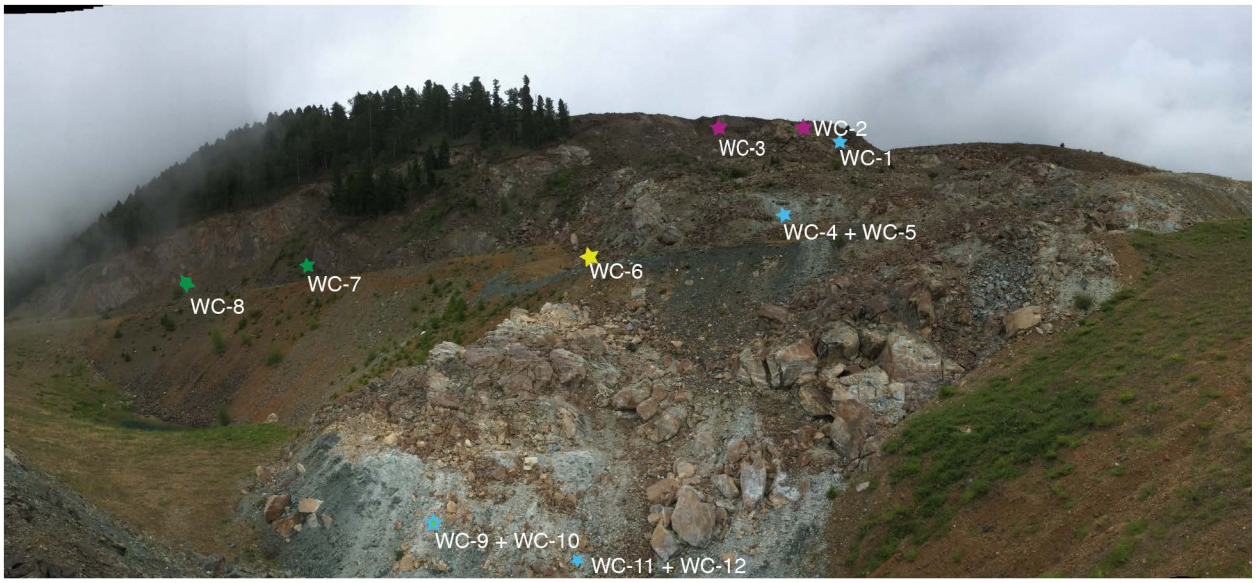

Figure 4: View of Willow Creek pit. Sampling locations are indicated by stars. Sample WC-13 is not denoted on this map.

Figure 5: Images showing samples at collection. Ruler or pocket knife for scale. Please refer to Table 1 for more sample descriptions.

Table 1: Sample descriptions and mineral estimates by XRD. Additional trace minerals identified by thin sections.

Sample Number	Sample Description	Location	Carbonate or Silicate Rich	Talc	Clinochlore	Chlorite	Calcite	Dolomite	Lizardite	Olinve (Forsterite)	Biotite (Phlogopite)	Pyrite	Minerals by Thin Section (<2%)
				Major Minerals						*Trace Minerals*			
WC 1	Talc veinlets - flaky talc	Main Talc Zone	Silicate	80%	15%	5%							CPX[a]
WC 4	Bulk talc replacing parent texture	Main Talc Zone	Silicate	95%	5%								Dolomite
WC 5	Weathered Marble	Main Talc Zone	Carbonate		20%		10%	70%					Biotite
WC 6	Dark waste material - chlorite marble	Chloritic Alteration Zone	Silicate	8%	2%	90%							Monazite
WC 7	Coarse grained banded marble (dolomitic)	Unaltered Marble Zone	Carbonate				20%	60%	4%	11%	5%		
WC 8	Scarp marble	Unaltered Marble Zone	Carbonate	7%			25%	61%	5%		2%		
WC 9	Gray microcrystalline talc	Main Talc Zone	Silicate	99%	1%								
WC 10	Green microcrystalline talc	Main Talc Zone	Silicate	95%	5%								
WC 11	Talc marble	Main Talc Zone	Carbonate	56%			35%	6%				3%	Opaque Mineral[b]
WC 12	Talc complete replacement of marble	Main Talc Zone	Silicate	98%	2%								
WC 13	Marble - talc vein contact	Outside Main Pit	Silicate	100%									Dolomite

[a] CPX - Clinopyroxene

[b] Opaque Mineral could possibly be pyrite.

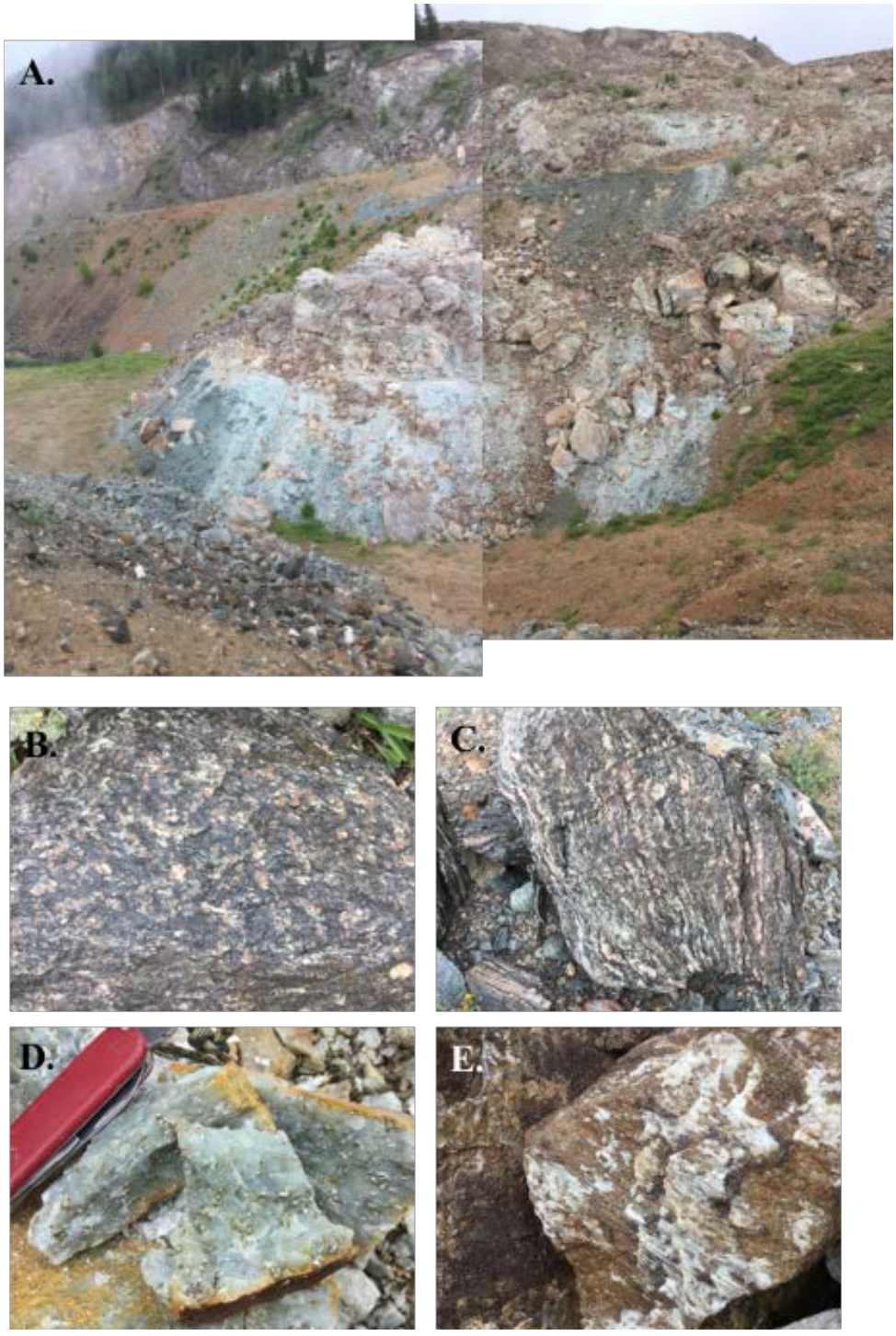

Figure 6: Field images of various locations from the mine. A) View from hanging wall of the pit. Footwall is composed of dolomitic marble and talc ore. B) Boulder of Dillion Gneiss with garnet or garnet relics. C) Banded gneiss boulder seen in lower boulder field. D) Talc with large pyrite crystals. WC-11 also contained pyrite but not with euhedral crystals of this scale. E) Large boulder of marble with slickenlines in talc showing movement along fault surface.

3.2 MINERAL IDENTIFICATION BY XRD

Mineral identification by X-ray Diffraction (XRD) was performed at RJ Lee Group, Inc. Samples were crushed using a McCrone Mill to reduce the sample into a sub-micron particle size powder. Approximately 15 grams of each sample were crushed, and the McCrone Mill was cleaned with isopropyl alcohol in between the crushing of each sample. A PANalytical X'Pert Pro Diffractometer using copper radiation equipped with an X'celerator RTMS (Real Time Multiple Strip) was used to carry out the XRD analysis using a silt size of 0.0635 at 40 mA and 45 kV over a full scan from 4-64° 2θ. Data reduction was performed using High Score Plus running COD, ICDD, and PDF+4 databases.

3.3 GEOCHEMICAL ANALYSIS

X-ray Fluorescence Spectroscopy (XRF) was performed on splits of the whole rock powders for major and minor element at the Peter Hooper Geochemical Lab at Washington State University. A low (2:1) Li-tetraborate fusion preparation method was use, and the samples were run on a ThermARL X-Ray Fluorescence Spectrometer (Johnson et al., 1999). In addition to XRF, the Peter Hooper Geochemical Lab performed trace elemental analysis using ICP-MS on the whole rock powders. Samples were prepared using a low-dilution fusion with di-lithium

tetraborate and analyzed on a Agilent 7700 ICP-MS with integrated sample introduction system (Johnson et al., 1999).

Based on the data received from the above analyses, four samples with greater that 50% carbonate minerals were chosen for acetic acid leaching. A split of 500-1000 mg of powdered sample was mixed with 1 M acetic acid at an approximately 50:1 fluid-rock ratio. Samples were set on a shaker table for eight hours. After being centrifuged (10 min. at 4000 rpm), the dissolved carbonate fraction was pipetted off and evaporated to dryness, then redissolved in 2% HNO_3. An aliquot of this solution was sent to Activation Labs (ActLabs) for analysis by ICP-MS for trace elements, and the remainder processed for Sr/Nd isotopes.

3.4 ISOTOPIC ANALYSIS

The leftover dissolved carbonate solution was spiked with tracer solution containing precisely known amounts of ^{87}Rb, ^{84}Sr, ^{147}Sm, and ^{150}Nd to determine concentrations by isotope dilution. Solutions were evaporated on a hot plate until dry and then reconstituted in 1.5 N HCl. Separation of Rb-Sr and REE from the matrix was carried out using cation exchange columns, and Sm-Nd was separated from other REEs using columns containing LnSpec® resin, eluted with dilute HCl.

A Milestone Ethos UP microwave digestion system was used to dissolve pure talc samples and those with less than 10% carbonate. During this digestion HCl, HNO_3 and HF were added to the samples and digested at 225°C for 30 minutes. Aqua Regia was then used to

dissolve any leftover fluorides from the samples. The samples were spiked with the Rb-Sr and Sm-Nd isotope tracers, and column separations were carried out as above.

Once separated, solutions were evaporated to dryness. For Sr isotope measurement, approximately 500 nanograms (ng) of separated Sr were loaded in 2N HNO_3 with Ta oxide on a single rhenium filament. For Rb analysis by isotope dilution, 1-10 ng of Rb was loaded in 1.0 N HCl on a single Re filament. For Nd isotope analysis, approximately 150 ng of Nd was loaded using 1.0N HCl on a double rhenium filament. For Sm analysis by isotope dilution, approximately 100 ng of Sm was loaded the same way as Nd. Samples were run on a Thermo-Finnigan MAT 262 multicollector thermal ionization mass spectrometer (TIMS) at the University of Pittsburgh. During Sr and Nd analyses, concentrations by isotope dilution were determined simultaneously with isotope compositions. For Sr isotope analyses, multiple standards of SRM 987 were run with each set of samples and all ratios corrected using these runs to a mean lab value of 0.71024. For Nd isotope analyses, La Jolla Nd standards were run repeatedly, yielding a calculated chondritic $^{143}Nd/^{144}Nd$ ratio of 0.511847.

4.0 RESULTS

4.1 FIELD RELATIONS AND MINERALOGY

The deposit outside of Alder, MT known as the Willow Creek deposit was active for only a short period of time from 1970-1979 (Berg, 1979). The deposit today is unrecognizable from what it would have looked like during active mine operations (**Figs. 4, 5**). The original ore is no longer visible and only "pods" or "pockets" of talc are seen throughout the boulder field. The talc that is still *in situ* is present in thin laminated layers or fingers within the marble. Talc is also present in several hydrothermal thin veins, 5-10 cm thick. Apparent thickness of these 5-10cm talc veins could be meters thick depending on orientation. It is green-gray in color, platy, or in some cases microcrystalline. The talc contains evidence of slickenlines (**Fig. 5E**) indicating sheer fractures. These slickenlines appear only on the soft surface of the talc and could also be conduits for fluid movement. Other evidence for fluid movement includes the numerous fractures containing mineralized talc presented in the mine as large veins or veinlets, as well as the presence of quartz veins and veinlets throughout the mine and a possible calcite vein within the slumped material (M. Sanchez, personal communication). The contact between the talc and the carbonate banded marbles is gradational. The fresh surface of the marble is white with pockets of a platy mineral, either biotite or chlorite, while the weathered surface is reddish.

This is can best be seen in the field photo of WC-7 (Fig. 6B) where the fresh surface and weathered surface can both be seen. Waste material is still present on the lower benches but none of it is in place in the inferred upper benches of the pit. The far side of the pit still has evidence of the paragneiss reported to be on the hanging wall by Berg (1979). Within the waste material, two boulders were observed which could possibly be the Dillion Gneiss (**Fig. 5B, C**). In one boulder (**Fig 5B**), relic garnets were observed within a gneissic matrix; in the other (**Fig. 4C**) tightly folded gneissic banding was observed with the pinkish mineral being reported as feldspar (M. Sanchez, personal communications). The position of each sample collected for this study is shown in **Figure 4**. The only sample not present on this map is sample WC-13, as it was not collected in the pit. Samples WC-2 and WC-3 are from mineralized veins not associated with the talc; these veins consist primarily of sepiolite and were not analyzed any further in this study. These sepiolite occurrences were only observed in the marble units and it is unknown if they cross cut the talc.

The overall mineralogy, in which the great majority of the samples were either talc or dolomite, is summarized in **Figure 7** and **Table 1**. The mineral percentages reported are based on XRD and thin section observations; individual XRD scans are provided in Appendix A. Six samples contained >70% talc. In these samples, accessory minerals were mainly chlorite and/or clinochlore. WC-1 also contained clinopyroxene as an accessory mineral. Four samples, WC-5, 7, 8 and 11, were chosen for leaching based on their relatively large carbonate (dolomite and calcite) component. WC-11 also contained small amounts of pyrite observed by thin section and XRD. An example of talc-associated pyrite from the lower bench boulder field is shown in **Figure 5D,** except this sample has larger euhedral crystals than those in WC-11. Sample WC-11 may represent the contact between the talc and carbonate

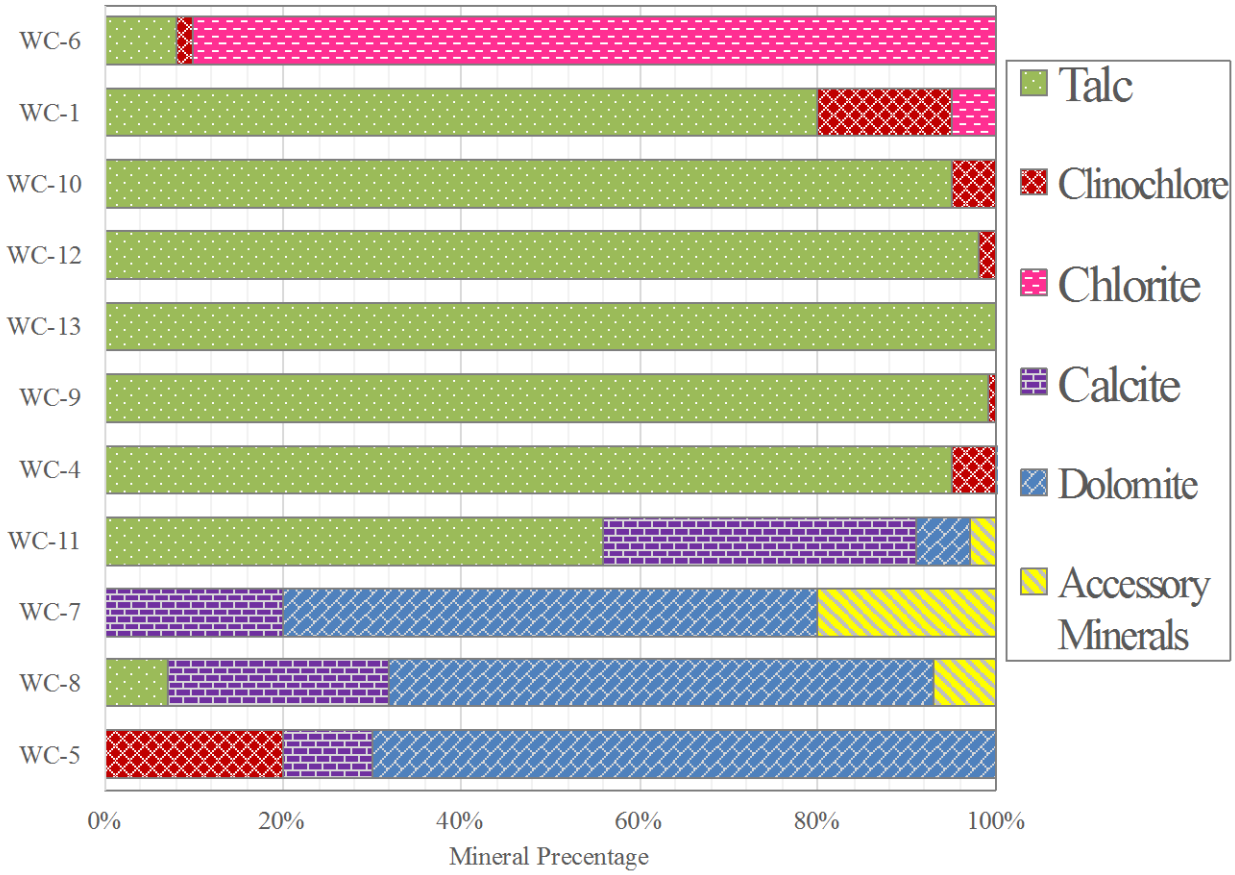

Figure 7: Overview of mineralogy as determined by XRD. Additional minerals were observed by thin section but with concentrations too low to detect by XRD. Please refer to Table 1 for these minerals. Additionally refer to Appendix A for XRD scans.

units. In thin section, the boundaries between the talc and the carbonate were sharp (Fig 8C). In some cases, the original rhombohedral shape of the carbonate was maintained but in most cases the talc is seen as a veinlet texture infiltrating between the carbonate grain boundaries. This pattern was observed in larger scale at the mine. Samples WC-7, WC-8, and WC-5 were dominated by carbonate minerals (primarily dolomite) as determined by XRD. Samples WC-7 and WC-8, which were located outside of the talc ore zone (**Fig. 4**), contained

massive lizardite usually in association with olivine. This lizardite occurrence was restricted to these samples and was detected by XRD and thin section. WC-7 also still preserves forsterite olivine with lizardite replacing the olivine rims (Fig. 8B). WC-5 and WC-7 also contained small amounts of biotite. Olivine, lizardite and biotite were found mainly in association with the dolomitic marble. In contrast Berg (1979) reported these minerals within the calcitic marble. This study did not find any evidence of these minerals within the calcitic marble. WC-6 was collected from the dark waste material within the mine, and is not *in situ*. This sample contains more than 90% chlorite and clinochlore with only about 10% talc present. In thin section, less than 1% monazite can be seen, which would be not be enough to be detected by XRD**.**

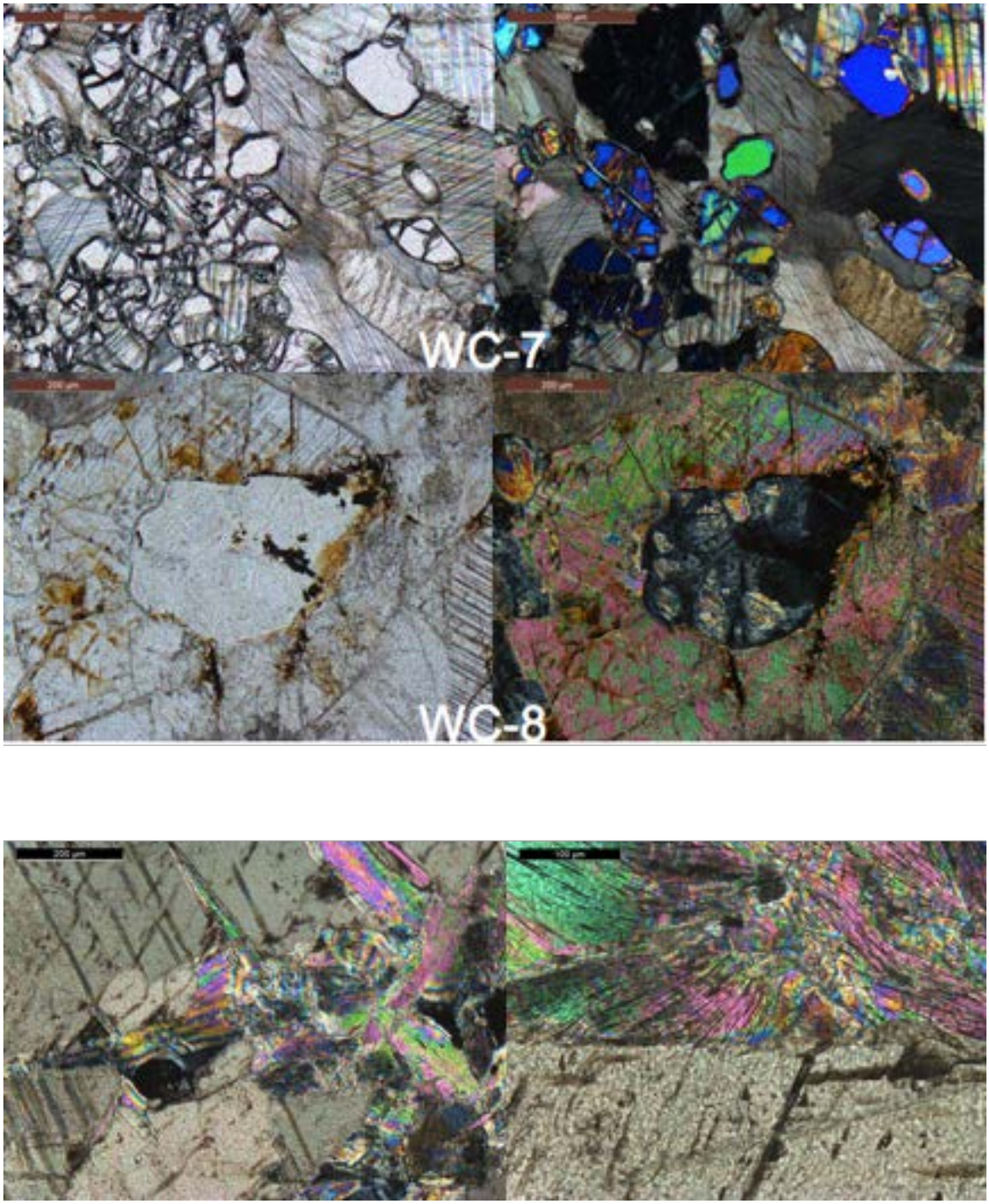

Figure 8: Thin section petrographic photomicrographs. A) Relic olivine grains surrounded by carbonate. B) Relic olivine grain completely replaced by serpentine and surrounded by carbonate. C) Vein talc between carbonate grains.

4.2 MAJOR AND TRACE ELEMENT VARIATIONS

Whole rock major element compositions of the samples from this study are presented in **Table 2**. To illustrate the compositional endmembers, the combined values of FeO +MgO+CaO are plotted against SiO_2 + Al_2O_3 for all samples in (**Fig. 9)**. Samples that are predominantly carbonate (WC-5, 7, 8 and 11) plot together to define one endmember, and the others plot in a trend extending from a mafic-intermediate silicate endmember toward the carbonate-rich endmembers. Interestingly, the two silicate-rich samples that extend the most toward the carbonate endmembers (WC-6 and WC-10) do not have XRD-detectable carbonate (**Fig. 7**). These samples also contain anomalously high contents of Th and U (**Table 3**).

Table 2: Major element composition (in wt. %) of rocks and leachates analyzed in this study

Sample	SiO_2	TiO_2	Al_2O_3	FeO[a]	MnO	MgO	CaO	Na_2O	K_2O	P_2O_5	LOI[b]	Total
Whole rock[c]												
WC-1	61.1	0.0315	0.797	1.07	0.0039	31.0	0.0474	<*dl*[d]	<*dl*	0.00284	5.38	99.4
WC-4	59.2	0.0568	1.79	1.92	0.0094	30.5	0.145	<*dl*	<*dl*	0.0626	6.10	99.8
WC-5	4.28	0.0290	0.623	2.13	1.02	17.0	31.7	<*dl*	0.0041	0.0255	40.9	97.7
WC-6	31.5	0.399	17.8	6.74	0.0742	29.6	0.0966	<*dl*	<*dl*	0.244	12.5	99.0
WC-7	7.10	0.0150	0.340	1.93	1.11	17.3	32.5	<*dl*	0.0529	0.00070	39.0	99.4
WC-8	2.53	0.0190	0.413	1.66	1.16	13.3	36.4	0.147	0.0704	0.00200	42.0	97.7
WC-9	62.6	0.0021	0.0810	0.988	0.0051	31.0	0.111	<*dl*	<*dl*	<*dl*	4.81	99.6
WC-10	40.7	0.314	12.8	5.28	0.0710	30.3	0.0368	<*dl*	<*dl*	<*dl*	10.5	100.0
WC-11	5.38	<*dl*	0.0462	0.443	0.334	4.70	47.3	<*dl*	<*dl*	<*dl*	39.5	97.7
WC-12	61.6	0.0269	0.366	1.78	0.0078	30.3	0.175	0.0342	<*dl*	0.0381	5.20	99.5
WC-13	62.6	0.0039	0.0429	1.06	0.0065	31.0	0.0378	<*dl*	<*dl*	<*dl*	5.27	100.0
HOAc leachate (carbonate)[e]											CO_2[f]	
WC-5	0.182	0.0042	0.040	0.85	0.88	14.5	35.0	0.022	0.015	–	44.4	96.0
WC-7	0.69	0.003	0.021	0.58	0.65	8.7	28.6	0.009	0.031	–	32.7	71.9
WC-8	0.267	0.0051	0.044	0.82	0.92	9.8	38.2	0.015	0.100	–	41.7	91.8
WC-11	0.388	0.0068	0.014	0.40	0.32	3.3	40.1	0.011	<0.01	–	35.5	80.1

[a]All Fe reported as FeO.

[b]LOI = Loss on ignition.

[c]Whole rock concentrations determined by XRF at Washington State University.

[d]<*dl* = below detection limit.

[e]Leachate concentrations determined by ICP-MS at ActLabs LLC. Concentration is normalized to the mass leached (assumed to be calcite/dolomite). P_2O_5 and LOI not determined.

[f]Wt. % CO_2 calculated assuming all Fe^{2+}, Mn^{2+}, Mg^{2+} and Ca^{2+} occurs as carbonate minerals.

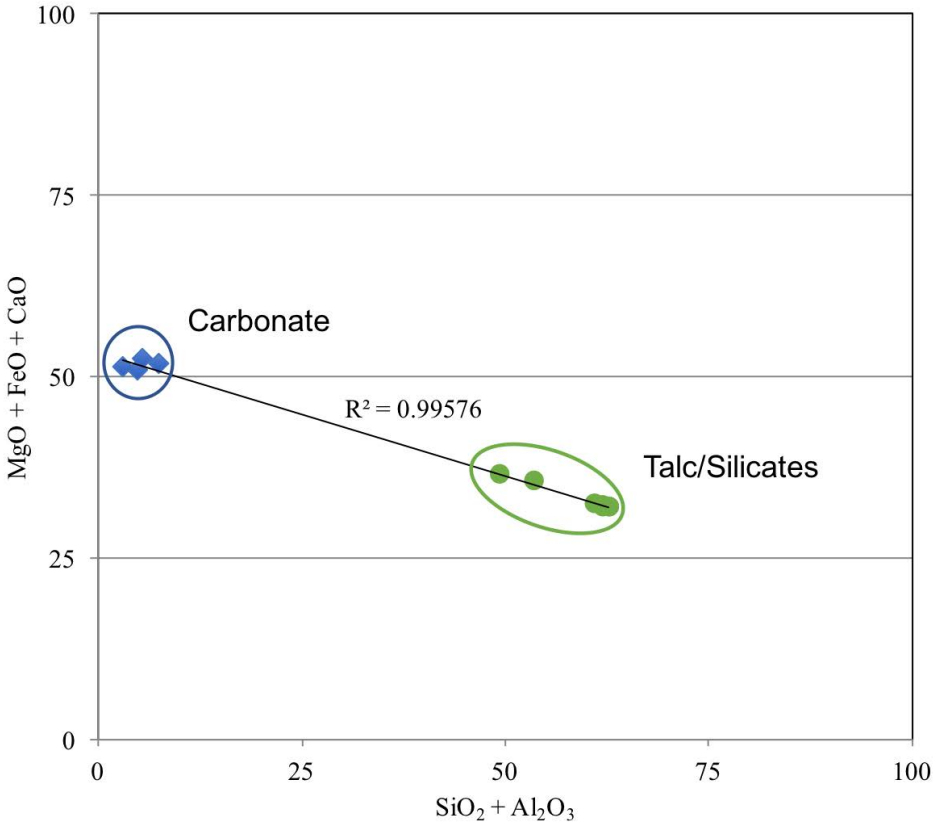

Figure 9: Major elements of carbonate rich vs. silicate rich whole rock samples. Carbonate is in blue diamonds and silicate is in green circles.

Table 3: Concentration of selected trace elements (in ppm) of whole rock and acetic acid leachates. REE reported in Table 4.

Table 3. Concentrations of selected trace elements (in ppm) of whole rock and acetic acid leachates. REE reported in Table 4.

Sample	Ba	Co	Cu	Cs	Ga	Hf	Nb	Ni	Pb	Rb	Sc	Sr	Ta	Th	U	Y	Zn	Zr
Whole rock[a]																		
WC-1	0.609	*n.m.*[b]	*n.m.*	0.205	*n.m.*	0.207	0.573	*n.m.*	0.203	0.333	0.494	0.512	0.0485	0.495	0.325	0.339	*n.m.*	3.39
WC-4	0.714	*n.m.*	*n.m.*	0.234	*n.m.*	0.571	1.40	*n.m.*	0.371	0.417	0.653	0.785	0.173	0.287	0.175	0.757	*n.m.*	4.20
WC-5	9.60	*n.m.*	*n.m.*	0.344	*n.m.*	0.153	0.375	*n.m.*	1.37	1.00	0.271	48.2	0.0375	0.600	0.333	3.19	*n.m.*	7.19
WC-6	0.931	*n.m.*	*n.m.*	0.216	*n.m.*	23.4	16.1	*n.m.*	6.21	0.375	0.896	1.12	0.683	49.2	6.02	56.9	*n.m.*	0.584
WC-7	11.0	*n.m.*	*n.m.*	0.145	*n.m.*	0.0941	0.236	*n.m.*	0.531	2.09	1.31	40.4	0.0460	0.367	0.186	2.10	*n.m.*	18.2
WC-8	16.3	*n.m.*	*n.m.*	0.213	*n.m.*	0.124	0.263	*n.m.*	5.77	2.63	0.820	74.7	0.0284	0.342	0.221	17.9	*n.m.*	5.59
WC-9	0.210	*n.m.*	*n.m.*	0.0855	*n.m.*	0.0114	0.0370	*n.m.*	0.125	0.143	6.23	0.452	0.00329	0.0716	0.0761	0.671	*n.m.*	114
WC-10	0.209	*n.m.*	*n.m.*	0.531	*n.m.*	3.423	12.5	*n.m.*	0.388	0.525	8.39	0.470	1.39	4.34	1.94	32.7	*n.m.*	0.347
WC-11	0.829	*n.m.*	*n.m.*	0.0146	*n.m.*	0.0191	0.0186	*n.m.*	0.328	0.148	7.60	123	0.00579	0.0162	0.216	61.3	*n.m.*	893
WC-12	0.368	*n.m.*	*n.m.*	0.215	*n.m.*	0.156	1.46	*n.m.*	0.312	0.217	0.784	0.686	0.180	0.488	0.320	1.10	*n.m.*	5.28
WC-13	1.67	*n.m.*	*n.m.*	0.0511	*n.m.*	0.0300	0.130	*n.m.*	0.170	0.0989	0.336	0.338	0.0226	0.288	0.187	0.318	*n.m.*	1.01
HOAc leachate (carbonate)[c]																		
WC-5	11.1	1.43	5.75	0.126	0.550	0.00475	<0.015	4.02	1.21	0.670	<2.5	54.5	<0.0025	0.178	0.133	2.52	5.85	0.105
WC-8	8.69	0.333	2.17	0.043	0.384	<0.004	<0.025	2.52	0.401	0.754	<4.0	40.3	<0.0040	0.0349	0.0356	1.83	56.9	0.103
WC-8	34.9	2.55	3.11	0.044	3.25	0.0104	<0.025	13.8	5.06	2.33	<4.0	81.8	<0.0040	0.136	0.0797	17.7	46.9	0.132
WC-11	4.88	0.558	3.26	0.011	1.16	0.0206	<0.015	8.70	0.719	0.156	9.15	151	<0.0025	0.0168	0.387	35.0	181	0.090

[a]Whole rock concentrations determined by ICP-MS at Washington State University.

[b]n.m. = not measured.

[c]Leachate concentrations determined by ICP-MS at ActLabs LLC. Concentration is normalized to the mass leached (assumed to be calcite/dolomite).

The major element compositions of the acetic acid leachates are dominated by CaO and MgO, with subordinate FeO, MnO, and SiO_2. This is expected, as the acetic acid primarily targets carbonate phases (dolomite and calcite). When the Ca^{2+}, Mg^{2+}, Fe^{2+}, and Mn^{2+} are assumed to complex with CO_3 as carbonate phases, the totals for the leachates come up 4-28% short of the expected mass based on the weight of the residue after leaching (see CO_2 calculation in **Table 2**). The cause of this discrepancy is not known, but it could be due to uncertainty in the residual mass after total evaporation of the leachate. To be consistent, all major and trace element concentrations of the leachates reported here are based on the apparent mass leached, rather than the calculated totals.

4.3 RARE EARTH ELEMENTS

Whole rock and leachate rare earth element (REE) data are reported in **Table 4**. The whole rock chondrite-normalized REE patterns (**Figure 10**) show negative Eu anomalies, which are also present in Early Proterozoic metapelites from other areas within the MMT (Roberts et al., 2002). This anomaly is presumably inherited from the protolith which is why it is so wide spread in this region. Three of the four carbonate-rich samples (blue squares) show enrichment in light REE compared to heavy REE, while most talc-rich samples have fairly flat signatures. WC-6 (top pattern in **Figure 10**) is almost pure chlorite and very enriched in REEs compared to the other samples within the data set. This enrichment could be due to the presence of accessory monazite, which is highly enriched in light REE (Rubatto et al., 2001;

Table 4: Concentrations of rare earth elements (in ppm) of whole rock and acetic acid leachates.

Sample	La	Ce	Pr	Nd	Sm	Eu	Gd	Tb	Dy	Ho	Er	Tm	Yb	Lu
Whole rock[a]														
WC-1	0.0737	0.191	0.0258	0.145	0.0647	0.0229	0.0659	0.0101	0.0592	0.0117	0.0336	0.00527	0.0351	0.00590
WC-4	0.153	0.423	0.0686	0.349	0.150	0.0321	0.184	0.0323	0.154	0.0290	0.0852	0.0137	0.0958	0.0168
WC-5	1.35	2.55	0.311	1.28	0.271	0.0891	0.292	0.0484	0.321	0.0781	0.237	0.0346	0.223	0.0364
WC-6	903	1826	208	779	142	17.3	68.4	5.06	14.8	2.06	4.99	0.712	4.71	0.897
WC-7	1.61	3.18	0.384	1.50	0.281	0.0588	0.252	0.0369	0.210	0.0501	0.145	0.0210	0.129	0.0222
WC-8	7.77	14.4	1.79	7.47	1.84	0.495	2.30	0.332	1.96	0.411	0.977	0.117	0.617	0.101
WC-9	0.178	0.362	0.0516	0.214	0.0686	0.0129	0.0802	0.0129	0.0870	0.0211	0.0809	0.0143	0.104	0.0199
WC-10	1.32	2.82	0.366	1.59	0.934	0.347	3.03	0.767	5.47	1.20	3.44	0.491	3.00	0.441
WC-11	1.36	4.84	0.907	5.53	3.74	1.16	7.23	1.57	9.98	1.98	5.47	0.852	5.60	0.837
WC-12	0.127	0.319	0.0463	0.218	0.112	0.0313	0.167	0.0315	0.193	0.0378	0.114	0.0194	0.143	0.0231
WC-13	0.0718	0.136	0.0214	0.0869	0.0366	0.00874	0.0583	0.00946	0.0519	0.0124	0.0255	0.00409	0.0324	0.00580
HOAc leachate (carbonate)[b]														
WC-5	1.80	3.12	0.336	1.33	0.245	0.0720	0.237	0.0354	0.249	0.0590	0.173	0.0261	0.166	0.0283
WC-7	1.15	1.99	0.212	0.820	0.154	0.0360	0.151	0.0225	0.156	0.0363	0.117	0.0172	0.108	0.0179
WC-8	10.5	17.7	1.92	7.77	1.75	0.429	2.11	0.279	1.71	0.369	0.937	0.116	0.670	0.100
WC-11	1.90	5.13	0.794	4.41	2.34	0.955	4.23	0.789	5.33	1.10	3.25	0.543	4.05	0.704

[a]Whole rock concentrations determined by ICP-MS at Washington State University.

[b]Leachate concentrations determined by ICP-MS at ActLabs LLC. Concentration is normalized to the mass leached (assumed to be calcite/dolomite).

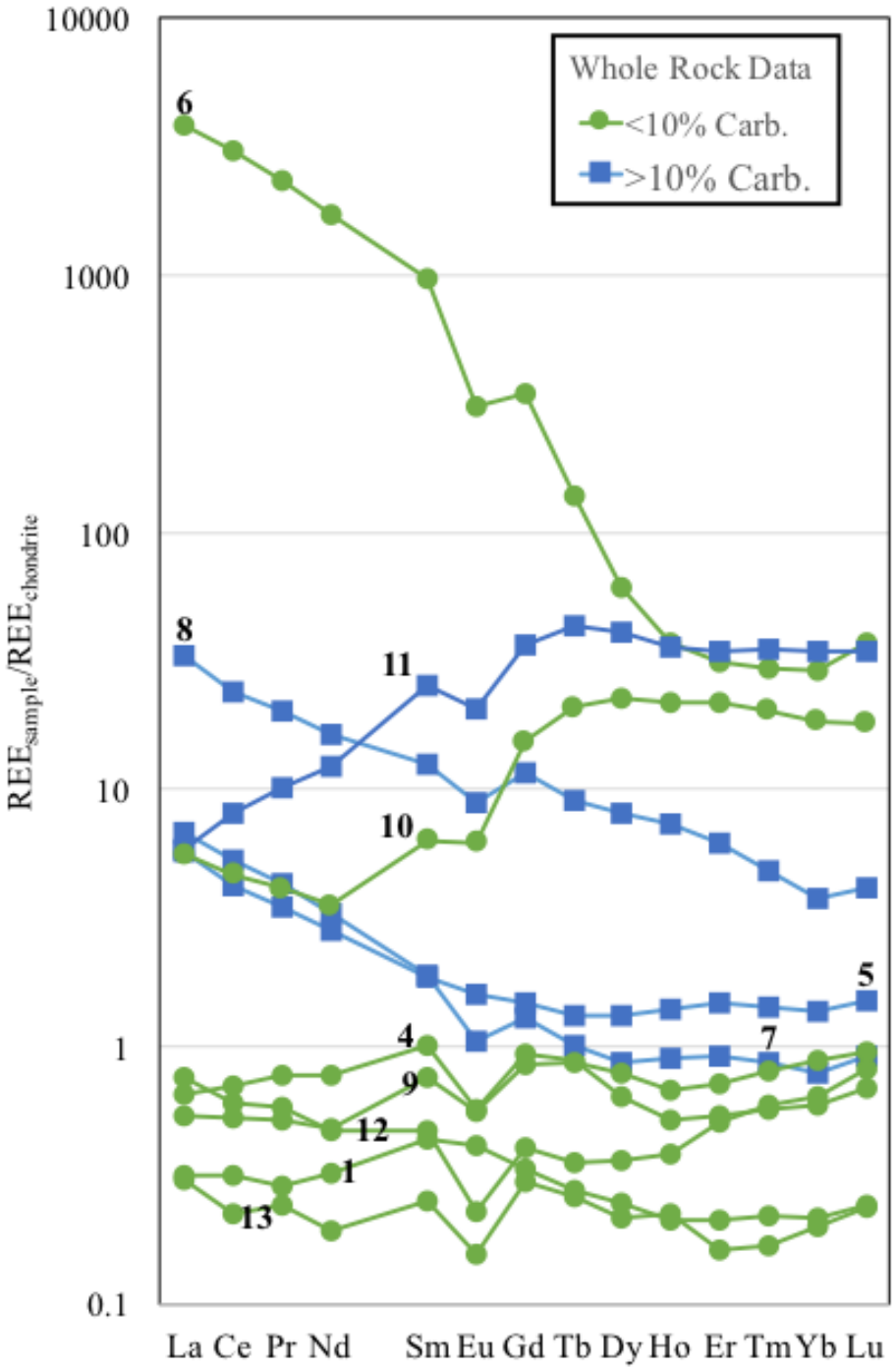

Figure 10: Chondrite-normalized whole rock REE patterns. Curves are labeled using samples numbers without location tag (WC-_).

Schaltegger et al., 1999). This would also be consistent with the high Th and U in this sample (Table3).

In contrast to the other three carbonate-rich samples, WC-11 is enriched in the heavy REE and depleted in light REE, although it has a similar negative Eu anomaly. This pattern is mirrored by silicate-talc sample WC-10, although the latter shows a small enrichment in the lightest REE. These two samples do not have any similarities in mineralogy but are both located in the main talc zone. For the carbonate-rich samples, the REE patterns of the leached carbonate are similar to the whole rock patterns (**Fig. 11**).

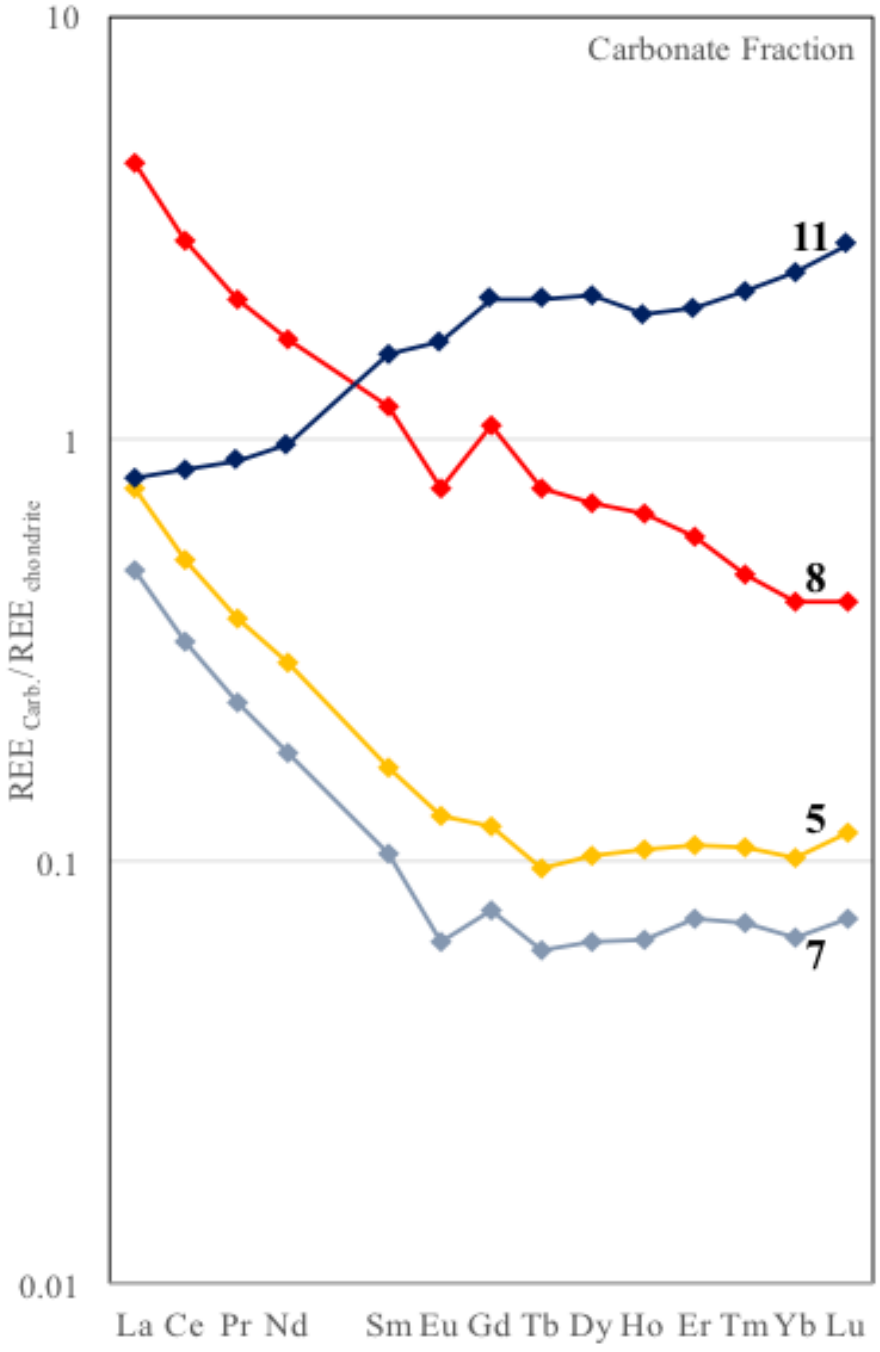

Figure 11: Chondrite-normalized HOAc leachate REE patterns. Curves are labeled using sample number without location ID (WC-_).

4.4 RADIOGENIC ISOTOPES

Rubidium-strontium and samarium-neodymium isotope data from the carbonate samples are presented in **Table 5**. Sm-Nd data were obtained from three samples, and Rb-Sr data from two. A plot of $^{147}Sm/^{144}Nd$ vs. $^{143}Nd/^{144}Nd$ ("isochron plot", **Fig. 14**) yields a linear correlation corresponding to an age of 1.42 ± 0.07 billion years (Ga), and an initial $\varepsilon_{Nd}(T)$ value of -18.1. The Rb-Sr data do not yield a meaningful isochron, and initial (1.42 Ga) $^{87}Sr/^{86}Sr$ values (0.72351 and 0.76373 for WC-5 and WC-8, respectively) vary significantly.

Table 5: Rb-Sr and Sm-Nd isotope data from carbonate leachates.

Sample	$^{87}Rb/^{86}Sr$[a]	$^{87}Sr/^{86}Sr$	$^{87}Sr/^{86}Sr(T)$[b]	$^{147}Sm/^{144}Nd$[a]	$^{143}Nd/^{144}Nd$	$\varepsilon_{Nd}(T)$[b]
WC-5	0.0381	0.723508 ± 0.000013	0.72273	–	–	–
WC-7	–	–	–	0.1358	0.510308 ± 0.000008	-19.03
WC-8	0.103	0.763730 ± 0.000020	0.76164	0.1418	0.510426 ± 0.000004	-17.80
WC-11	–	–	–	0.3363	0.512229 ± 0.000005	-18.07

[a]Based on isotope dilution measurement.
[b]For T = 1.422 Ga.

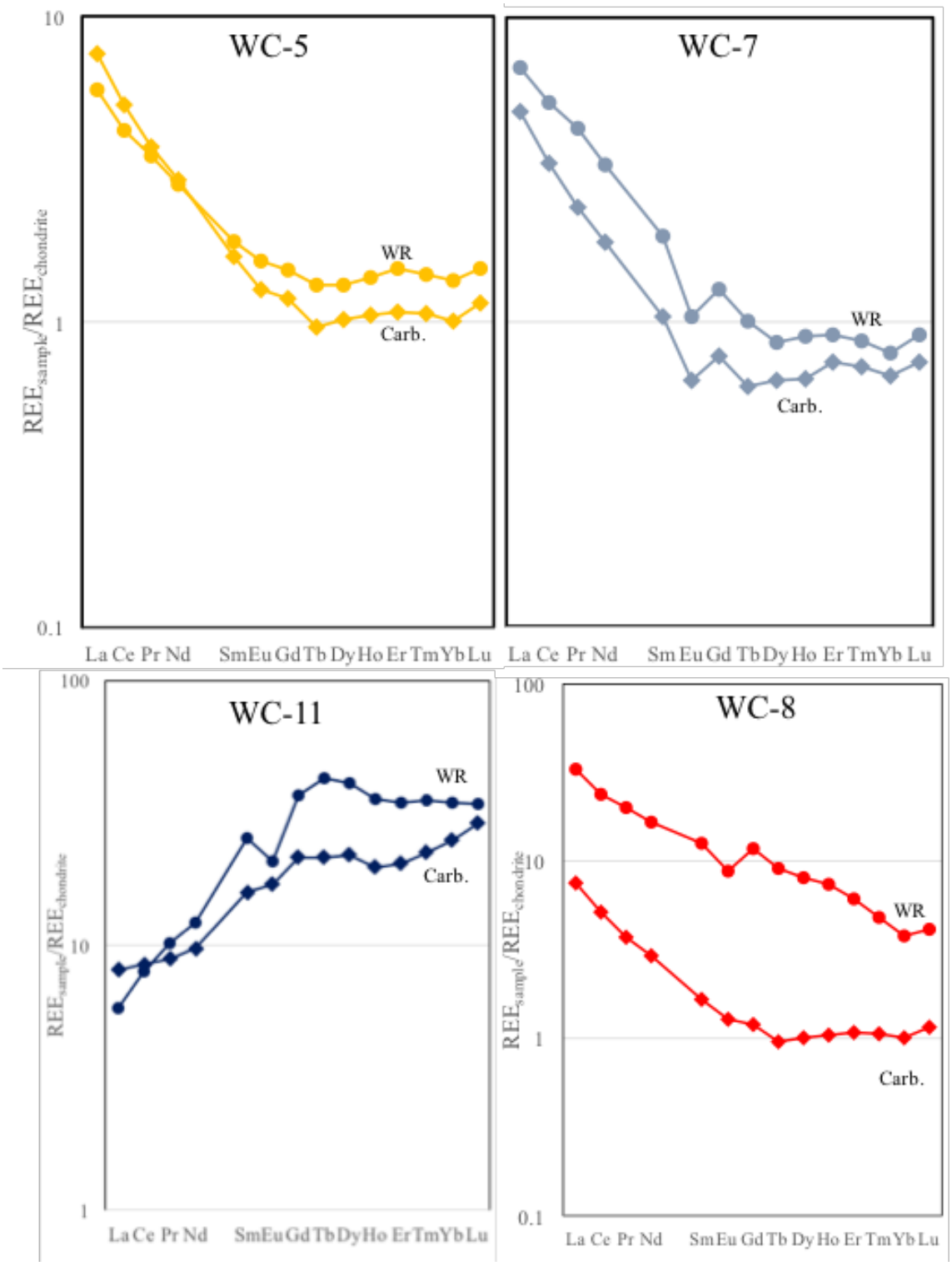

Figure 12: Comparison of whole rock and carbonate leach REE patterns for HOAc leached samples.

5.0 DISCUSSION

5.1 PARAGENESIS

The five samples containing relatively pure talc and low levels of SiO_2 and Al_2O_3 (WC-1, 9, 10, 12 and 13) yield REE patterns that are strikingly similar to each other, including slight negative Eu anomalies in four of them (**Fig. 10**), indicating that the talc all formed from the same source and event. This suggests that either 1) the talc inherited its major and trace elements from a relatively uniform carbonate source, or 2) that REE and talc components were transported with the hydrothermal fluid. The uniformity of the carbonate REE can be evaluated by the REE patterns of the carbonate leachates; three of these (the most dolomitic) have similar patterns, while the calcite-rich leachate (WC-11) shows a significantly different slope (**Fig. 11**). However, the three leachates that were analyzed for Sm-Nd isotopes, including WC-11, define an isochron that is entirely consistent with the inferred age of hydrothermal talc formation, suggesting that they were isotopically homogenized during this event. This implies at least meter-scale communication during the episode of talc formation, most likely facilitated by hydrothermal fluids. Moreover, the observation that carbonate from both the altered and unaltered zone yields similar $\varepsilon_{Nd}(T)$ values suggests that the carbonate itself is the source of the REE (and of the Mg for talc), rather than an overprinting hydrothermal fluid. The negative Eu anomaly was most likely inherited from the carbonate source.

Brady et al. (1998) measured δD and $\delta^{18}O$ values from three deposits also within the talc corridor, including the Treasure and Regal Mines (**Fig. 3**). Their study indicated that the talc was out of isotopic equilibrium with the surrounding host carbonate, and they concluded that the hydrothermal events were localized within specific fault zones. The REE patterns present in this study suggest that talc samples from different parts of the Willow Creek Mine are actually in equilibrium with each other, potentially homogenized by the same hydrothermal event.

5.2 SOURCE OF TALC COMPONENTS AND FLUID

Basinal or connate water(s) from the Belt Basin and/or Lemhi Subbasin are likely the most important fluids for the formation of talc in Southwest Montana (Brady et al., 1998; Underwood, 2016). To look at the carbonate as a potential source for the talc mineralizing components we used samples WC-7 and WC-8 from the unaltered marble zone (**Fig. 4**) as examples of the marble before the talc event occurred, and compared these samples to our 90% or greater talc samples (**Fig. 13**). The talc is significantly depleted in light REE and/or enriched in heavy REE compared to the carbonate. At present, the equilibrium partitioning of REE between carbonate minerals and talc at hydrothermal temperatures is not known, but these data suggest that the lighter REE with their larger ionic radii are excluded more strongly than heavier, smaller REE from the octahedral Mg site in talc. Conversely, the light REE may be accepted more readily into the carbonate lattice relative to talc.

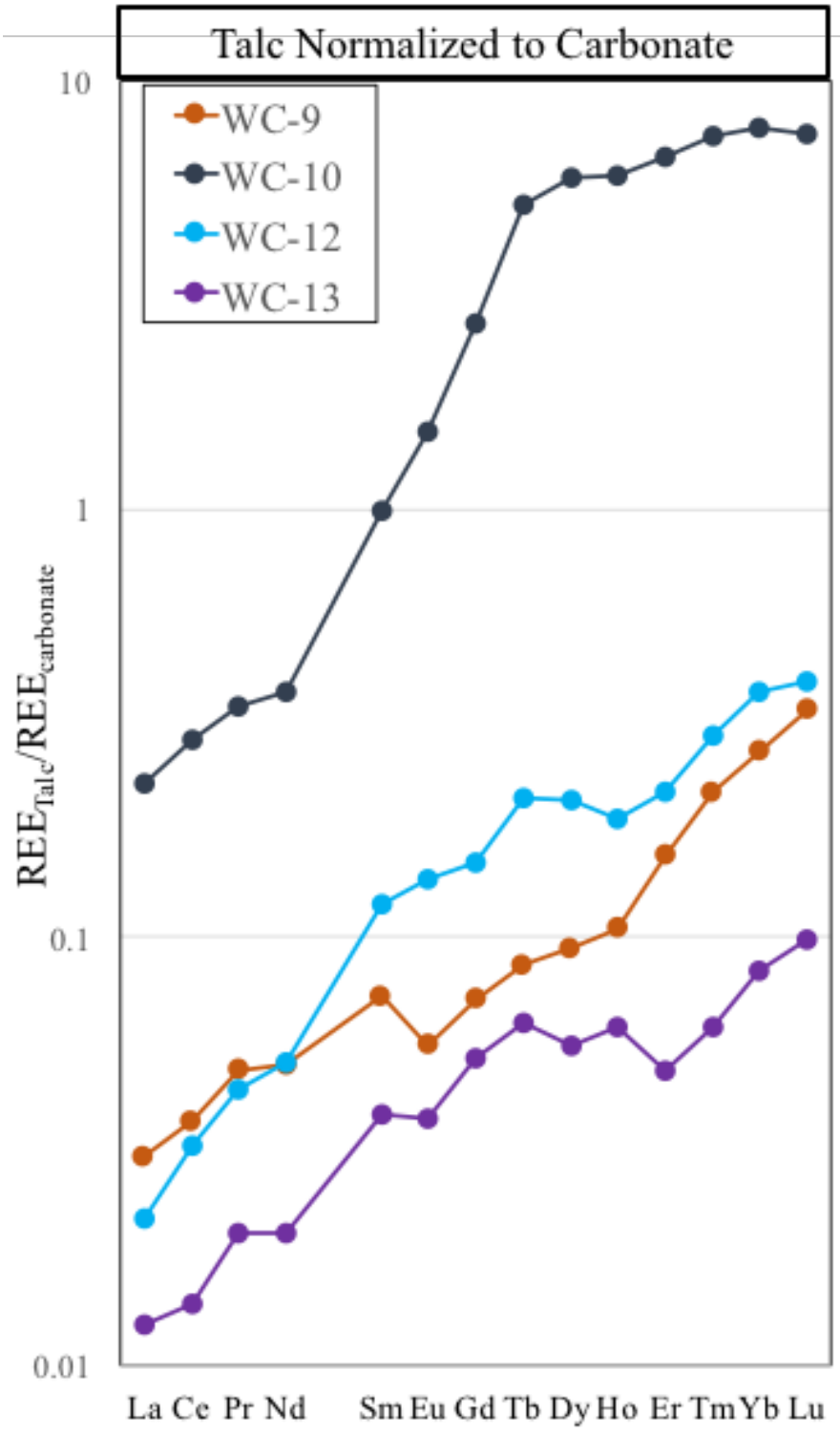

Figure 13: REE patterns of four talc pure samples normalized to the average carbonate fraction pattern of two unaltered marble samples.

Gammons and Matt (2002) studied fluid inclusions in quartz associated with talc from two nearby deposits: Yellowstone and Cadillac. They determined that the hydrothermal fluids were highly enriched in $CaCl_2$ and roughly 7x saltier than modern seawater. They concluded that the deposits were formed by regional fluid migration due to Proterozoic rifting in association with the opening of the belt basin. This fluid composition is consistent with the findings of Migdisov et al. (2016) in their experimental REE mobility study within hydrothermal fluids.

These experimental data showed that chloride was one of the main ligands responsible for the transport of REEs in hydrothermal solutions (Migdisov et al. 2016). This study also noted that chloride species fractionate LREE more than HREE, meaning that LREE are more readily leached and transported within chloride rich hydrothermal fluids when compared to HREE (Migdisov et al. 2016). This is the opposite effect we see within our patterns, where the HREE are preferentially extracted out of the carbonate. This again argues that the HREE were preferentially extracted by talc over the LREE compared to carbonate.

The crack-seal veins of quartz within the Willow Creek suggest cyclic buildup of fluid pressure during the faulting activity. If there was extra silica in the fluid during the talc-forming event, it could have been pushed out into these veinlets to form the quartz veins (Collettini et al., 2009). Thus, the quartz fluid inclusions studied by Gammons and Matt (2002) would be directly related to the faulting event and hydrothermal fluid movement that mineralized the talc. Collettini et al. (2009) also noted that in the presence of silica-rich fluids, precipitation of calcite and talc could be caused by stress-induced dissolution of dolomite. In the Willow Creek deposit, calcite could be considered a byproduct of the recrystallization of dolomite to talc according to following the following reaction:

$$3\ MgCa(CO_3)_2 + 4\ SiO_2 + H_2O = Mg_3Si_4O_{10}(OH)_2 + 3\ CaCO_3 + CO_2 \quad (1)$$

dolomite silica talc calcite

In summary, we suggest that talc in the Willow Creek Mine formed during a hydrothermal event in which dolomitic carbonate reacted with fluids, liberating its magnesium to form talc. The talc inherited its rare earth elements primarily from the carbonate, while the silica needed for talc formation was carried into the system by the fluids. As talc mineralized excess calcium carbonate was crystallized as calcite. The presence of pyrite in the lower benches of the deposit suggest that there was extra iron in the system. The extra iron and the slight enrichment in LREE signal that the talc formed in a near-surface reducing supergene environement (Cerino et al., 2007; Migdisov et al., 2016). Near surface mineralization produces acidic solution and carries them downward in the system and reprecipates sulfides.

5.3 EVENT TIMING

Two stages of talc mineralization are thought to have contributed to the Willow Creek deposit (Anderson et al., 1990; Roberts et al., 2002). The first was a retrograde metamorphic event (M2) at ~1800 - 1700 Ma, and the second a later hydrothermal event (M3) (Brady et al., 2004; Roberts et al., 2002). This study did not find any isotopic or geochemical evidence to support the earlier event at ~1700 Ma, which was originally thought to be preserved in the calcitic marble. Olivine relics within the dolomitic marbles were the only indication of high metamorphism and replacement. It could be possible that

this event is only evident in the minerals of the Dillion Gneiss, which has been extensively studied (Anderson et al., 1990; Berg, 1979; Brady et al., 1998; Cerino et al., 2007; Cheney et al., 2004; Garihan, 1979; Roberts et al., 2002). $^{40}Ar/^{39}Ar$ from muscovite in the nearby Ruby Range supports this regional hydrothermal event, but the fluid evidently did not reach a high enough temperature to reset biotite and hornblende ages (~300°C and ~550° C, respectively) (Brady, 2004; Brady et al., 2004; Rollinson, 2014)

Sm-Nd isotope data (**Figure 14)** from the carbonate samples define a linear trend corresponding to an age of 1.42±0.07 Ga, which is consistent with the inferred age of the hydrothermal event responsible for the talc formation. This isochron is anchored by a calcitic marble point; which suggest that calcite mineralized during the same period as the talc. Previously calcitic marbles were thought to be older than the talc-forming event, but this study indicates otherwise. Another indication that the calcite is younger than the dolomite is that olivine, lizardite, and biotite were only noted in the dolomitic marble and not in association with the calcite.

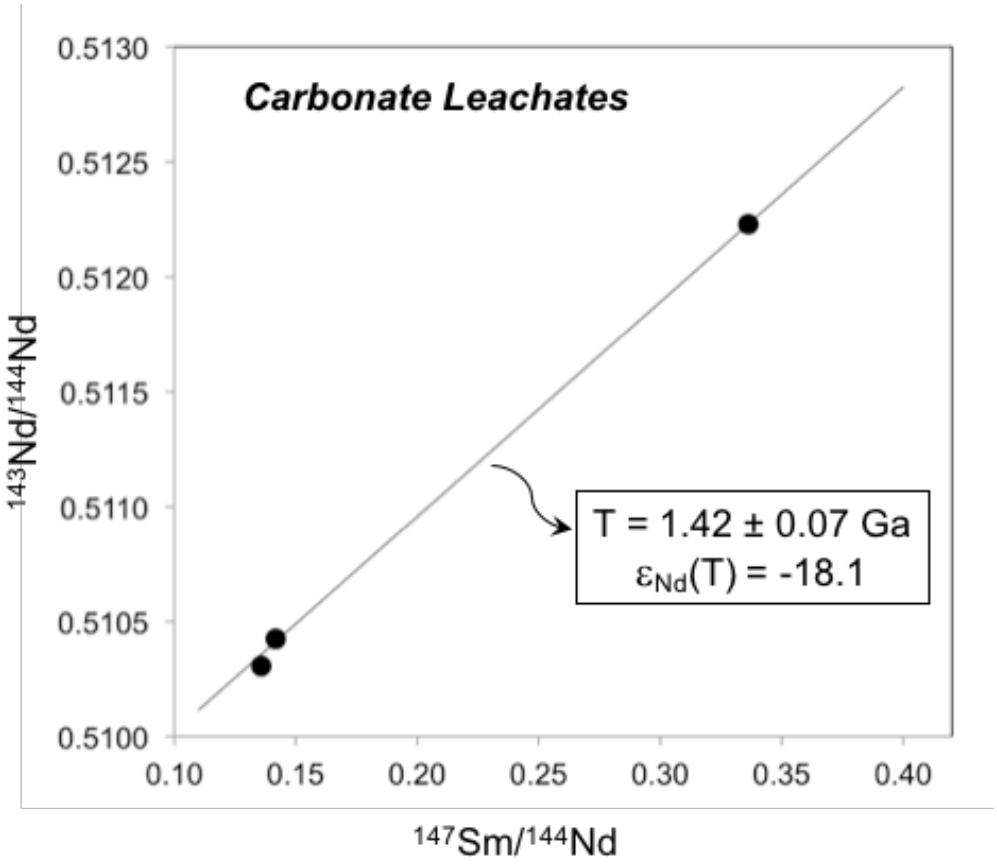

Figure 14: Sm-Nd isochron of the carbonate leachate. High $^{143}Nd/^{144}Nd$ - $^{147}Sm/^{144}Nd$ samples contains a high proportion of calcite, while the other two samples are dolomitic.

6.0 CONCLUSIONS

High purity talc mines southwestern Montana have provided and will continue to provide the majority of the United States talc; active mines are currently producing up to 400 KT of talc per year. This study provides petrographic, geochemical and isotopic constraints on the processes and timing of talc-forming events in the now-closed Willow Creek mine near Alder, Montana. The talc mineralized zone lies within a larger unaltered dolomitic marble complex. Petrographic study shows evidence of fluid flow and replacement of carbonate with talc, suggesting that the talc formed at the expense of pre-existing dolomitic marble. A samarium-neodymium (Sm-Nd) isochron from carbonate within and outside of the talc-mineralized zone yields an age of 1.42±0.07 Ga, which is consistent with previous estimates of the age of talc mineralization. This suggests that the carbonate was the major source of Sm and Nd (and therefore of other rare earth elements) that were distributed among the talc and residual carbonate, and that the talc formed (and obtained its Mg) primarily by a reaction with dolomite in which calcite is a by-product. Similar ε_{Nd} between the altered and unaltered carbonate indicates that REEs came from carbonate and were not a hydrothermal fluid overprint. I conclude that the petrogenesis of the Willow Creek talc deposit would conceivable minimized the mineralization of coexisting asbestiform minerals.

Most of the high-purity talc samples yield relatively flat chondrite-normalized REE patterns while the dolomitic marble is enriched in light REE. If the dolomite and talc were in

equilibrium (via hydrothermal fluid) during the talc-forming event, this would imply that talc has a stronger preference for the heavy REE (and/or excludes light REE) relative to carbonate. The hydrothermal fluid would have been a silica-rich, acidic fluid most likely sourced from basinal brine. Nearby intrusion into the Ruby and Tobacco Root mountains would have supplied the heat and faulting throughout the area provided conduits for the fluid movement.

APPENDIX A

XRD SCANS

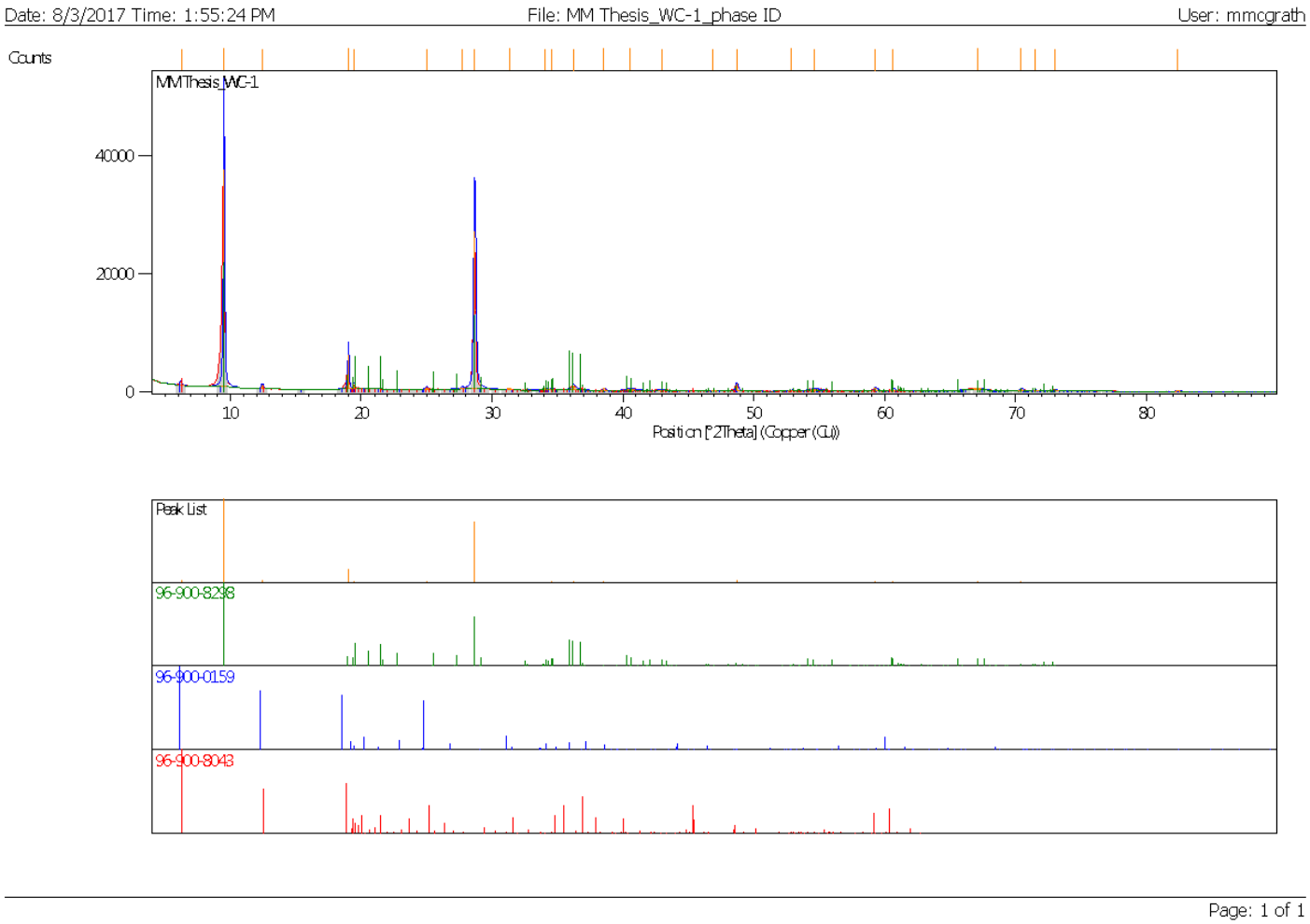

Scan 1: XRD Scan of WC--1

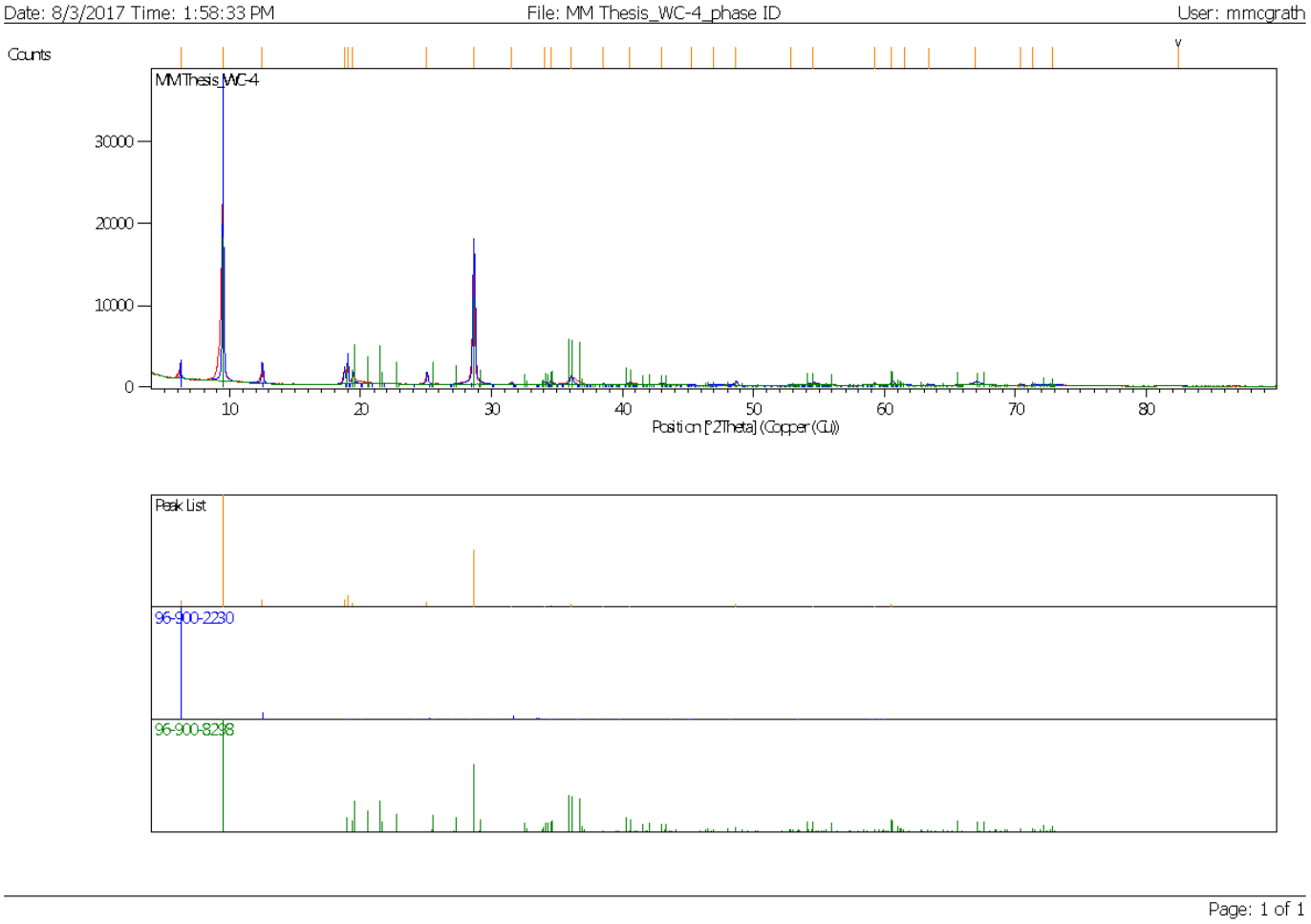

Scan 2: XRD Scan of WC-4

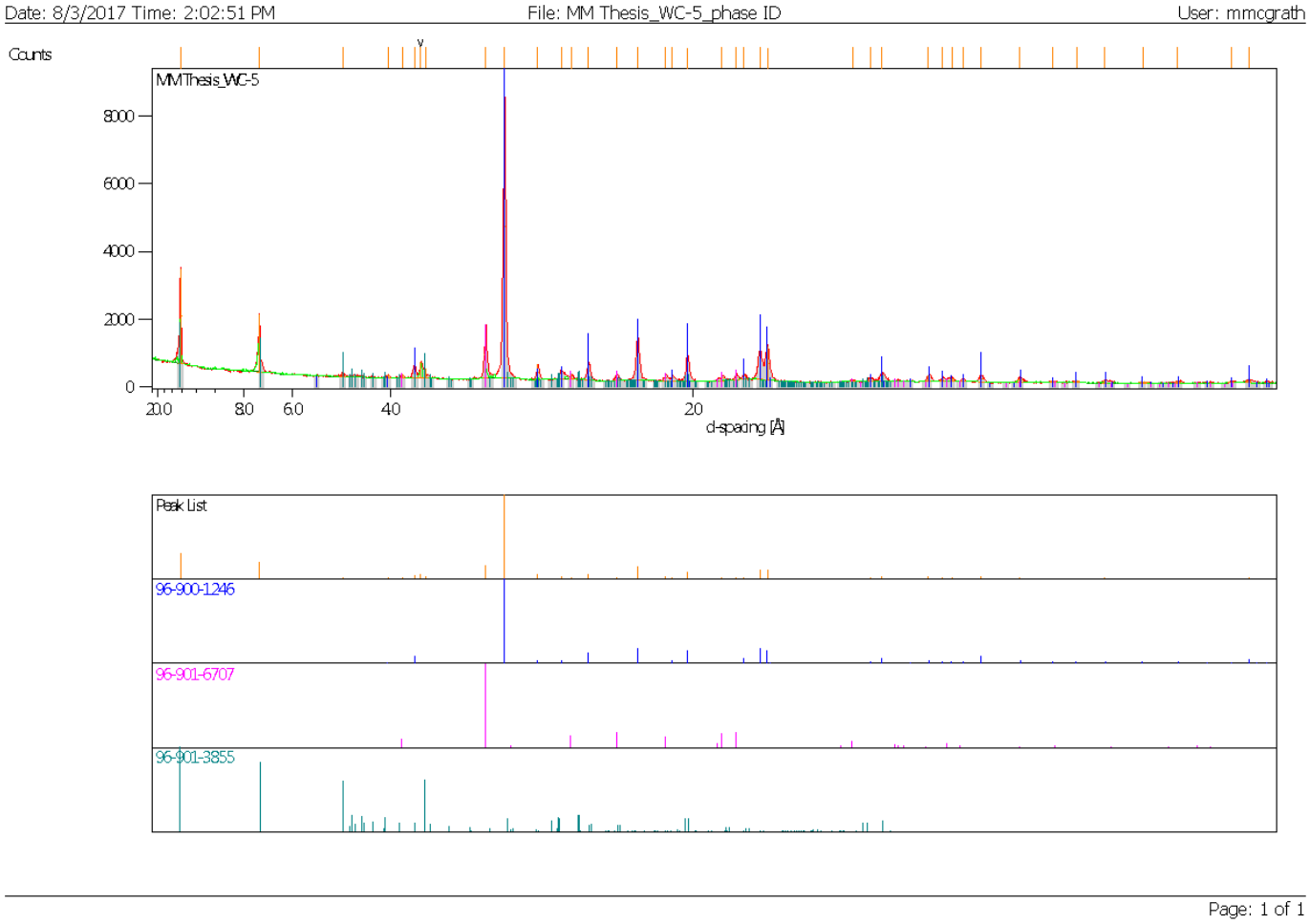

Scan 3: XRD Scan of WC-5

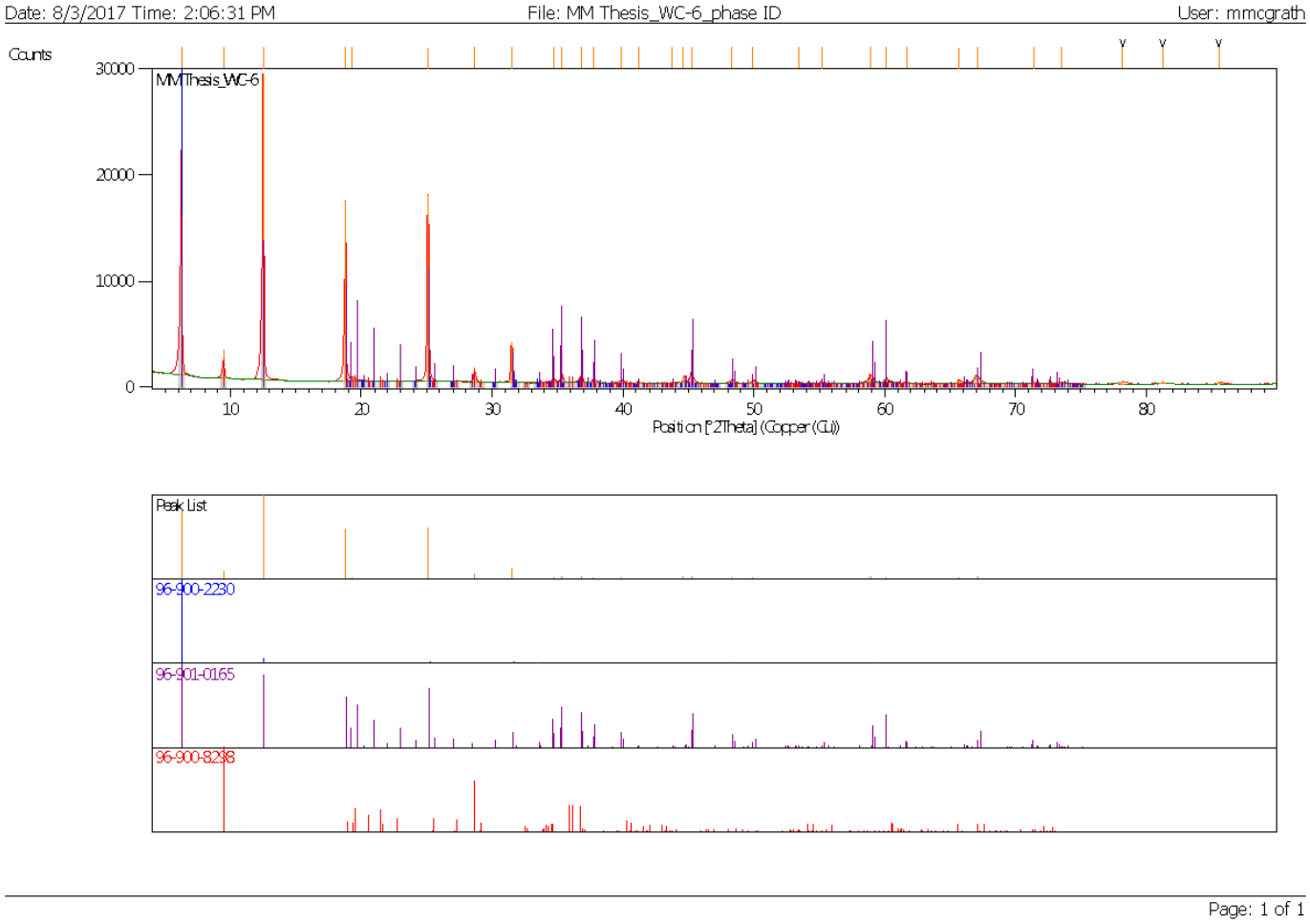

Scan 4: XRD Scan of WC-6

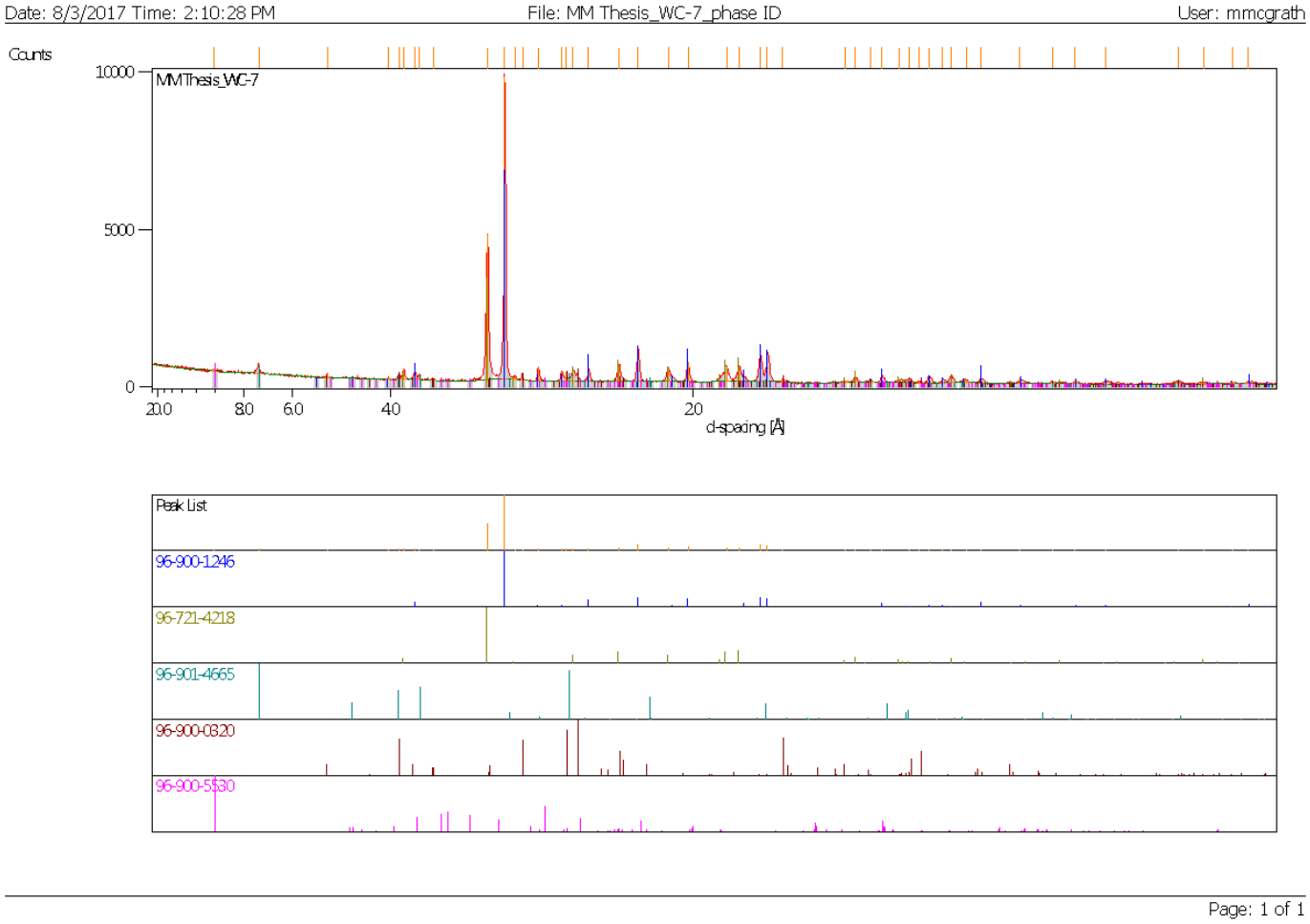

Scan 5: XRD Scan of WC-7

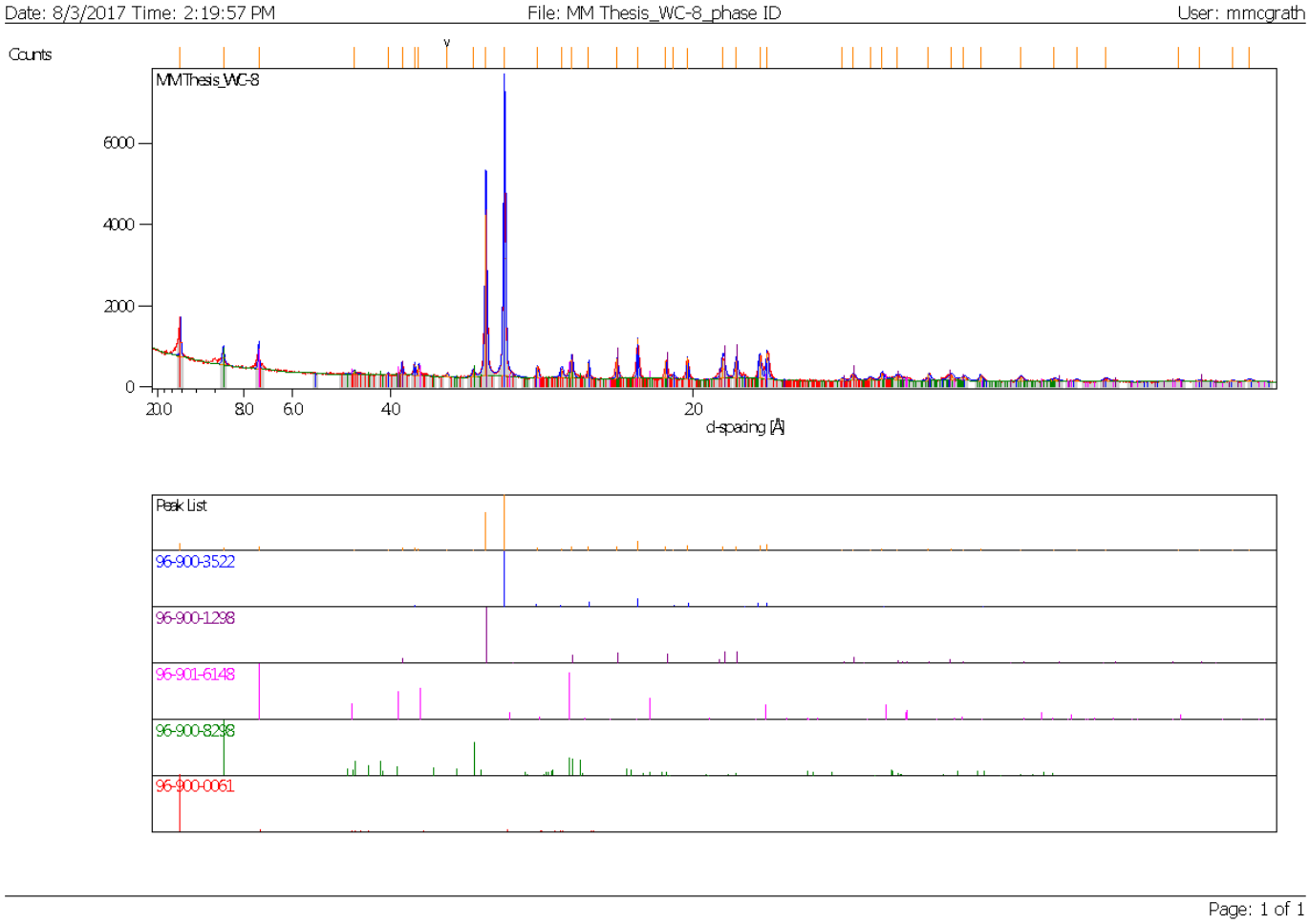

Scan 6: XRD of WC-8

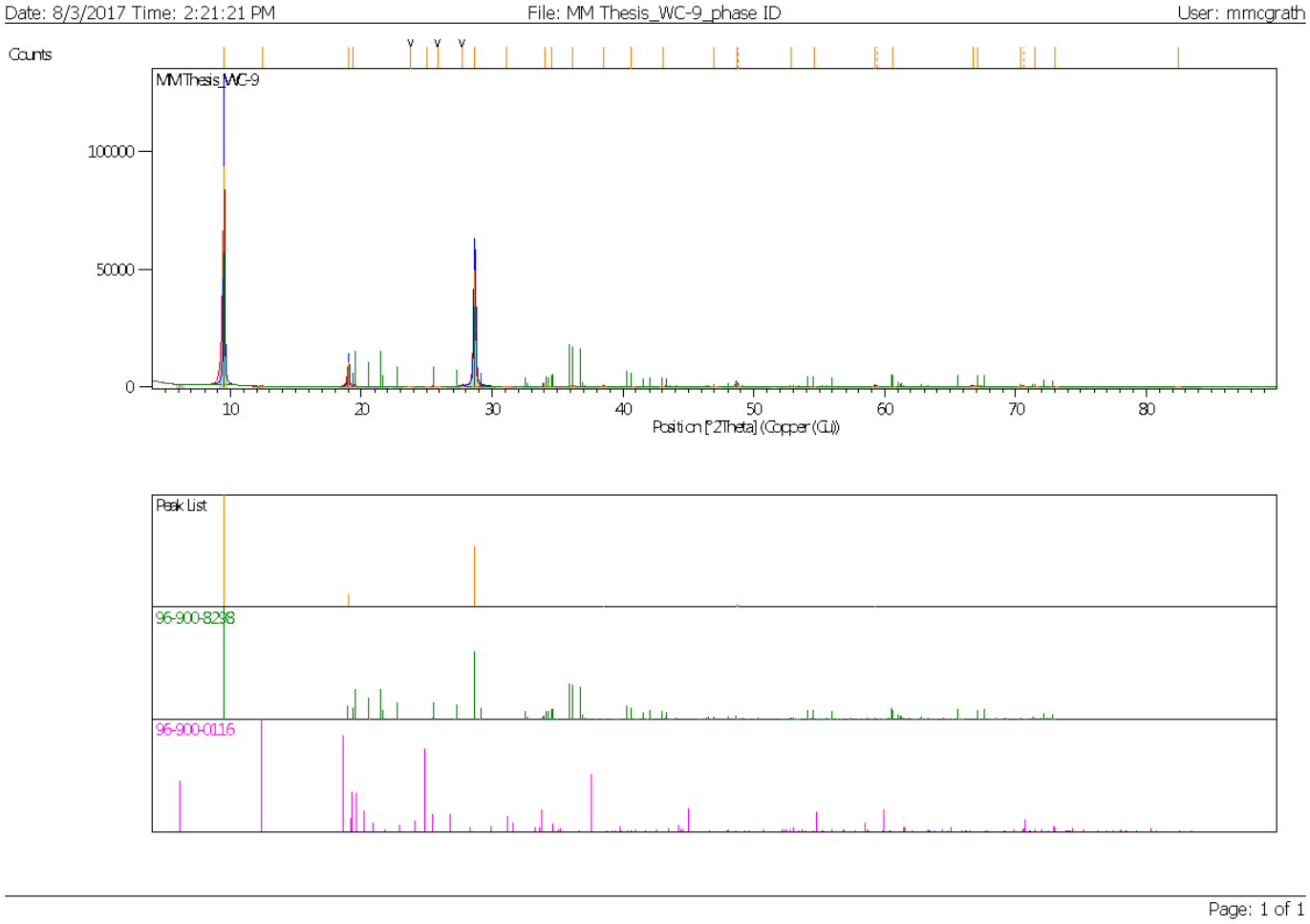

Scan 7: XRD Scan of WC-9

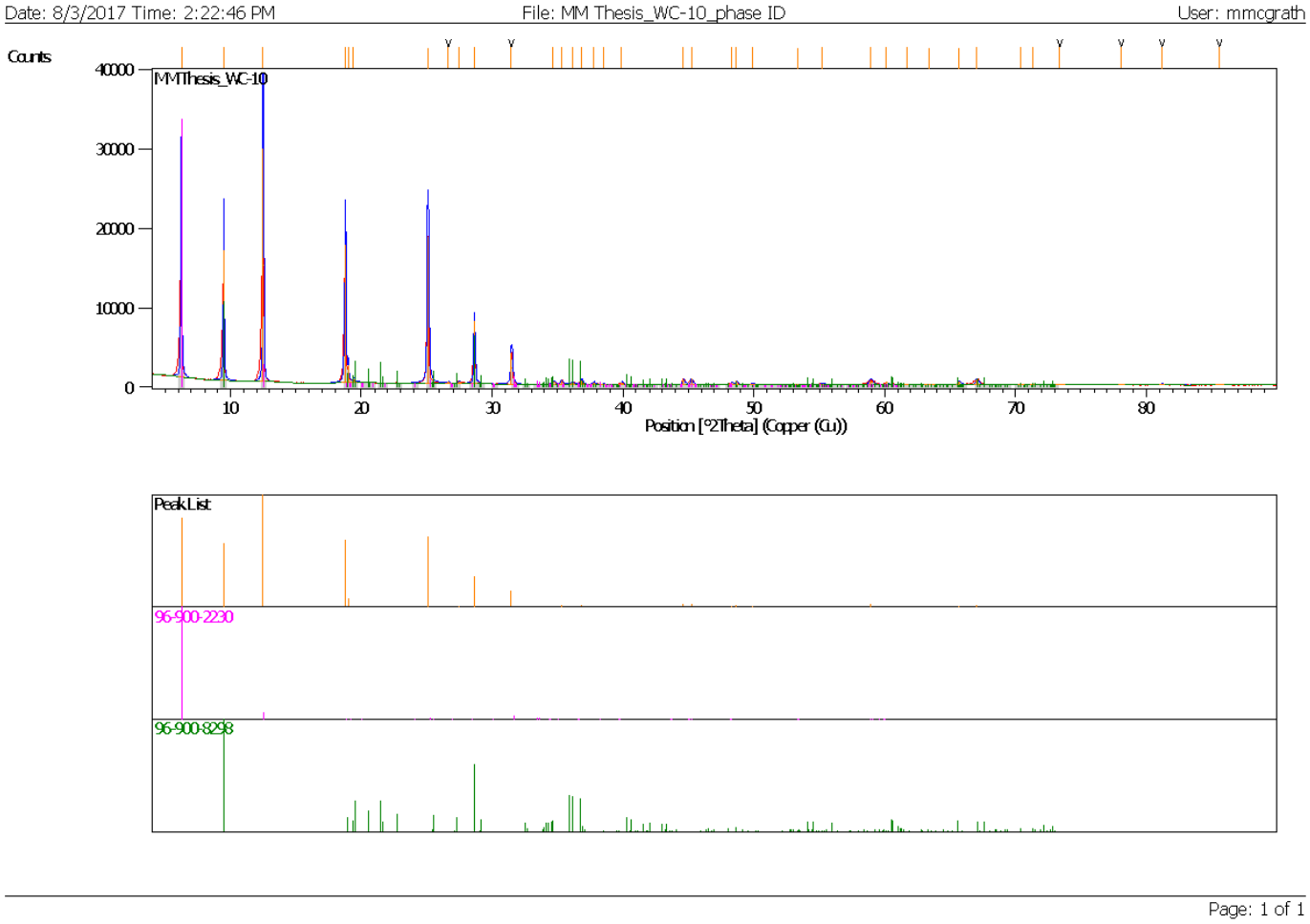

Scan 8: XRD Scan of WC-10

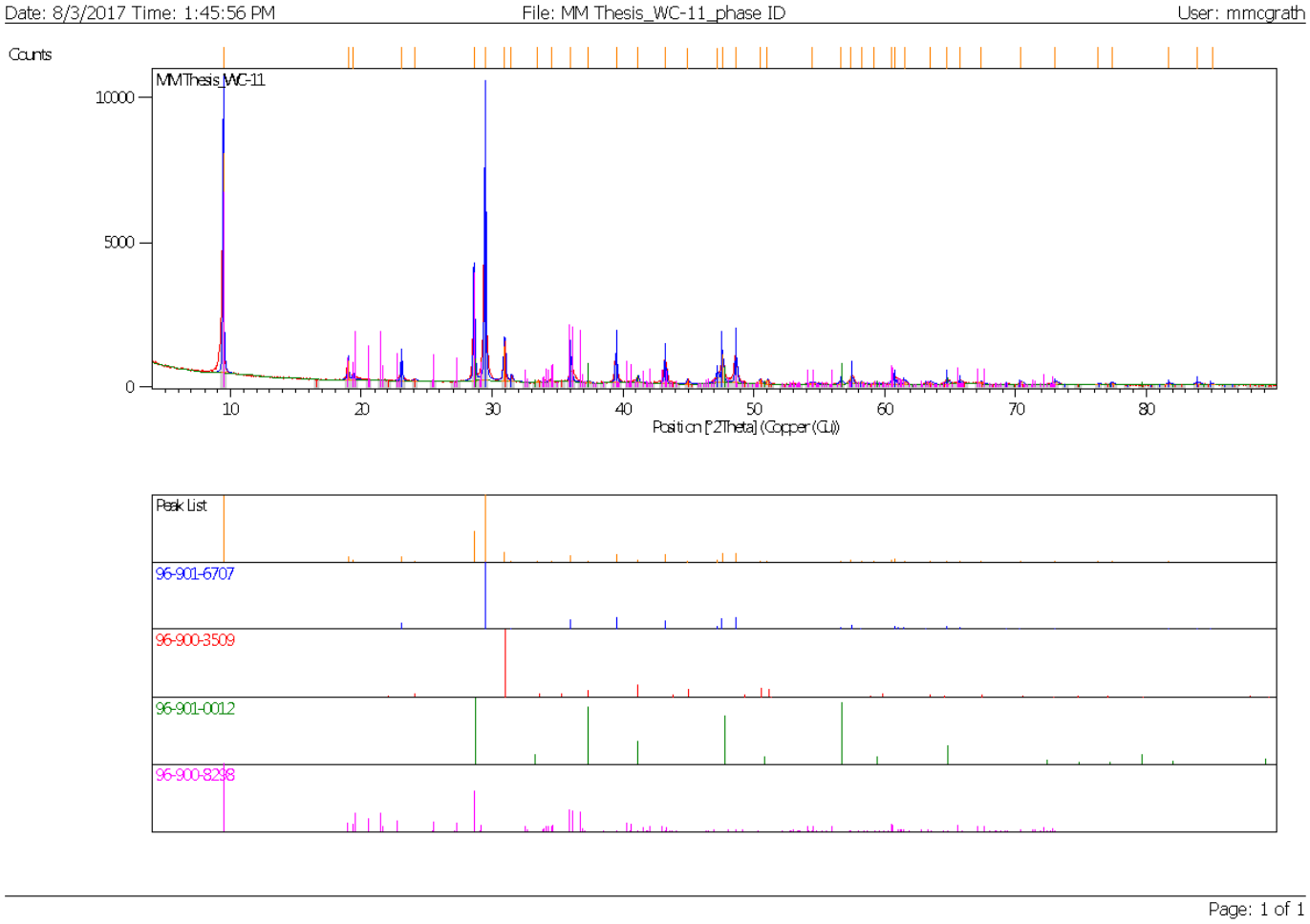

Scan 9: XRD Scan of WC-11

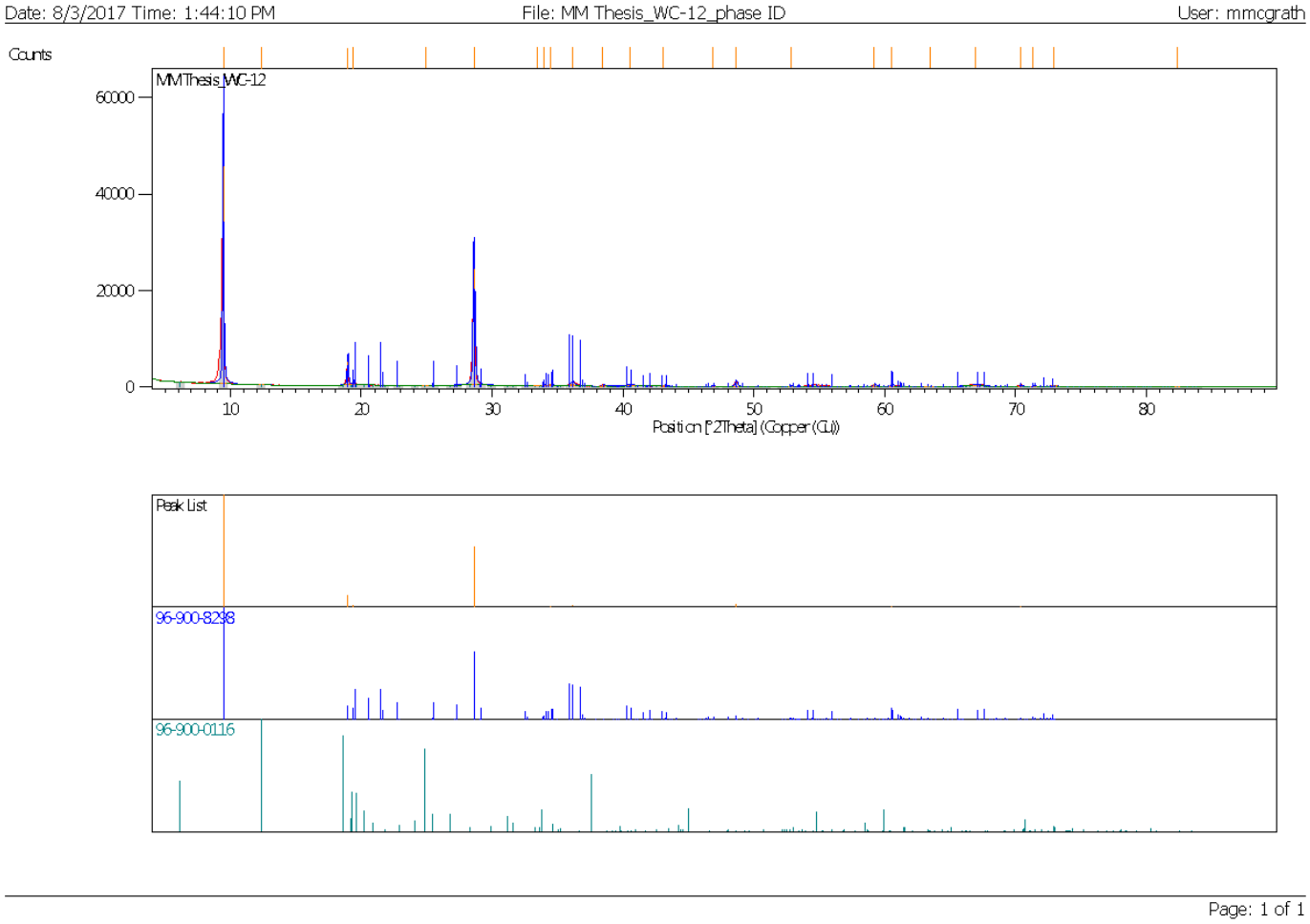

Scan 10: XRD Scan of WC-12

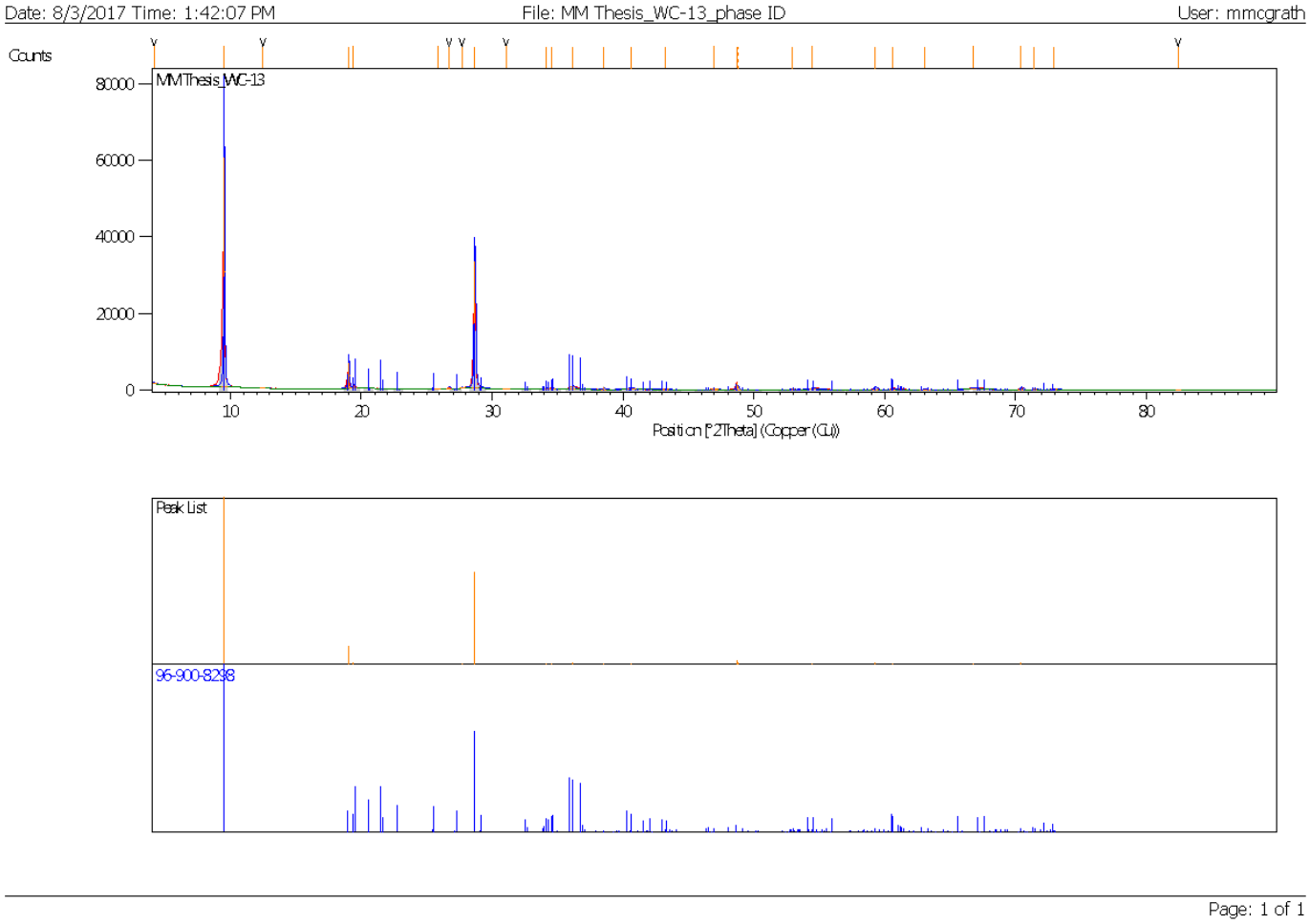

Scan 11: XRD Scan of WC-13

APPENDIX B

MINERAL PROPERTIES

Table 6: Properties and formulas of observed minerals.

Observed Mineral	Formula	Mineral Family	Crystal System	COD Database Number[a,b]
Calcite	$CaCO_3$	Carbonates	Trigonal	96-900-966
Dolomite	$CaMg(CO_3)_2$	Carbonates	Trigonal or Rhombohedral	96-900-3521
Talc	$Mg_3Si_4O_{10}(OH)_2$	Phyllosilicate	Monoclinic or Triclinic	96-900-8297
Tremolite/Actinolite	$Ca_2(Mg,Fe)_5Si_8O_{22}(OH)_2$	Inosilicate	Monoclinic	
Anthophyllite	$Mg_7Si_8O_{22}(OH)_2$	Inosilicate	Orthorhombic	
Chrysotile	$Mg_3Si_2O_5(OH)_4$	Phyllosilicate	Monoclinic	
Lizardite	$Mg_3Si_2O_5(OH)_4$	Phyllosilicate	Monoclinic	96-900-7424
Chlorite	$A_{5-6}T_4Z_{18}$[c]	Phyllosilicate	Monoclinic	96-901-0164
Clinochlore	$Mg_5Al(AlSi_3O_{10})(OH)_8$	Phyllosilicate	Monoclinic	96-900-2229
Olivine -Forsterite	Mg_2SiO_4	Nesosilicates	Orthorhombic	96-900-0319
Biotite- Phologpite	$KMg_3AlSi_3O_{10}(OH)_2$	Phyllosilicate	Monoclinic	96-900-5529
Clinopyroxene - Clinoferrosillite	Fe_2SiO_3	Inosilicate	Monoclinic	96-900-0917
Pyrite	FeS_2	Sulfide	Isotropic	96-901-0011
Monazite	$CePO_4$	Phosphate	Monoclinic	

[a] COD - Crystallography Open Database

[b] Number for minerals identified by XRD

[c] A- Mg, Fe, Mn, Na, Ni, Li, Al; B- Si, Al; Z - O, OH

BIBLIOGRAPHY

Akizuki, M., and Zussman, J. (1978) The unit cell of talc. Mine References ral. Mag. Citeseer.

Alcock, J., Muller, P., and Jercinovic, M. (2013) Monazite ages and pressure–temperature–time paths from anatectites in the southern Ruby Range, Montana, USA: evidence for delamination, ultramafic magmatism, and rapid uplift at ca. 1780 Ma. Canadian Journal of Earth Sciences, 50(11), 1069-1084.

Anderson, D.L., Mogk, D.W., and Childs, J.F. (1990) Petrogenesis and timing of talc formation in the Ruby Range, southwestern Montana. Economic Geology, 85(3), 585-600.

Berg, R. (1991) Geology of talc and chlorite deposits in Montana. Proceedings of the 27 th Forum on Geology of Industrial Minerals, Banff, Alberta, p. 1991-23.

Berg, R.B. (1979) Talc and chlorite deposits in Montana. Montana Bureau of Mines and Geology.

Boulvais, P., De Parseval, P., D'Hulst, A., and Paris, P. (2006) Carbonate alteration associated with talc-chlorite mineralization in the eastern Pyrenees, with emphasis on the St. Barthelemy Massif. Mineralogy and Petrology, 88(3-4), 499-526.

Brady, J. (2004) Precambrian geology of the Tobacco Root Mountains, Montana. Geological Society of America.

Brady, J.B., Kovaric, D.N., Cheney, J.T., Jacob, L.J., and King, J.T. (2004) 40Ar/39Ar ages of metamorphic rocks from the Tobacco Root Mountains region, Montana. Geological Society of America Special Papers, 377, 131-149.

Burger, H.R. (2004) General geology and tectonic setting of the Tobacco Root Mountains. Geological Society of America Special Papers, 377, 1-14.

Buzon, M., and Gunter, M.E. (2016) Current Issues with Purported "Asbestos" Content of Talc: Part 2, Examples in Hydrothermal Hosted Talc Ores. SME Annual Meeting, p. 11, Pheonix, AZ.

Cerino, M., Childs, J., and Berg, R. (2007) Talc in southwestern Montana. Introduction to the Geology of the Dillon Area: Northwest Geology, 36, 9-22.

Chen, C., Lu, A., Cai, K., and Zhai, Y. (2002) Sedimentary characteristics of Mg-rich carbonate formations and minerogenic fluids of magnesite and talc occurrences in early Proterozoic in eastern Liaoning Province, China. Science in China Series B: Chemistry, 45(1), 84-92.

Cheney, J.T., Brady, J.B., Tierney, K.A., DeGraff, K.A., Mohlman, H.K., Frisch, J.D., Hatch, C.E., Steiner, M.L., Carmichael, S.K., and Fisher, R.G. (2004) Proterozoic metamorphism of the Tobacco Root Mountains, Montana. Geological Society of America Special Papers, 377, 105-129.

Childs, J.F. (2016) The Talc Deposits of Southwestern Montana: An Overview. SME Annual Meeting, p. 16-140. Society of Mining and Engineering Phoenix, AZ.

Corona, J.C., Jenkins, D.M., and Dyar, M.D. (2015) The experimental incorporation of Fe into talc: a study using X-ray diffraction, Fourier transform infrared spectroscopy, and Mössbauer spectroscopy. Contributions to Mineralogy and Petrology, 170(3), 1-15.

Frost, B.R., Chamberlain, K.R., and Frost, C.D. (2003) Early Archean to Mesoproterozoic evolution of the Wyoming Province: Archean origins to modern lithospheric architecture. Canadian Journal of Earth Sciences, 40(10), 1357-1374.

Gammons, C.H., and Matt, D.O. (2002) Using fluid inclusions to help unravel the origin of the hydrothermal talc deposits in Southwest Montana Northwest Geology, 31, 44-53.

Gatta, G.D., Merlini, M., Valdrè, G., Liermann, H.-P., Nénert, G., Rothkirch, A., Kahlenberg, V., and Pavese, A. (2013) On the crystal structure and compressional behavior of talc: a mineral of interest in petrology and material science. Physics and Chemistry of Minerals, 40(2), 145-156.

Greenwood, W. (1998) A mineralogical analysis of fibrous talc. University of Maryland, College Park. MS Thesis, 162 pp.

Grexa, R., and Parmentier, C. (1979) Cosmetic talc properties and specifications. Cosmetics & Toiletries, 94, 29-33.

Gunter, M.E., Buzon, M., and McNamee, B.D. (2016) Current Issues with Purported "Asbestos" Content of Talc: Part 1, Introduction and Examples in Metamorphic and Ultramafic Hosted Talc Ores. SME Annual Meeting, p. 8, Pheonix, AZ.

Harben, P., and Kuzvart, M. (1996) Talc and soapstone. Industrial minerals: A global geology, 407-417.

Hecht, L., Freiberger, R., Gilg, H.A., Grundmann, G., and Kostitsyn, Y.A. (1999) Rare earth element and isotope (C, O, Sr) characteristics of hydrothermal carbonates: genetic implications for dolomite-hosted talc mineralization at Göpfersgrün (Fichtelgebirge, Germany). Chemical Geology, 155(1), 115-130.

Hutchison, J., Nissen, H.-U., and Wessicken, R. (1979) Observation of talc-tremolite interfaces by high resolution electron microscopy. Physics and Chemistry of Minerals, 4(3), 275-280.

Johnson, D., Hooper, P., and Conrey, R. (1999) XRF analysis of rocks and minerals for major and trace elements on a single low dilution Li-tetraborate fused bead. Advances in X-ray Analysis, v, 41, p. 843–867 Le Bas, MJ. Citeseer.

Joshi, P. (2009) Role of fluids in the formation of talc deposits of Rema area, Kumaun Lesser Himalaya.

Joshi, P., and Sharma, R. (2015) Fluid inclusion and geochemical signatures of the talc deposits in Kanda area, Kumaun, India: implications for genesis of carbonate hosted talc deposits in Lesser Himalaya. Carbonates and Evaporites, 30(2), 153-166.

Kesler, S.E. (1994) Mineral resources, economics, and the environment. Prentice Hall.

Klein, C., and Dutrow, B. (2008) The Manual of Mineral Science. John Wiley & Sons, Inc.

Larson, A. (1991) Talc formation in the Regal-Keystone mine of the Ruby Range. Dillon, Montana.

Linder, D.E., Wylie, A.G., and Candela, P.A. (1992) Mineralogy and origin of the State Line talc deposit, Pennsylvania. Economic Geology, 87(6), 1607-1615.

Mann, J.A. (1960) Geology of part of the Gravelly Range area, Montana.

McCarthy, E. (2015) The Talc Resources of the World a Historical Perspective. Society of Mining and Enigneering Annual Conference, Pheonix, AZ.

McCarthy, E. (2016) The Talc Resources of the World: A Historical Perspective. SME Phenoix, AZ.

McNamee, B.D. (2013) Characterization of Minerals: From the Classroom to Soils to Talc Deposits. ERIC.

Migdisov, A., Williams-Jones, A., Brugger, J., and Caporuscio, F.A. (2016) Hydrothermal transport, deposition, and fractionation of the REE: Experimental data and thermodynamic calculations. Chemical Geology, 439, 13-42.

Olson, R.H. (1976) The geology of Montana talc deposits. Montana Bureau of Mines and Geology Special Publication, 74, 99-143.

Roberts, H., Dahl, P., Kelley, S., and Frei, R. (2002) New 207 Pb–206 Pb and 40 Ar–39 Ar ages from SW Montana, USA: constraints on the Proterozoic and Archæan tectonic and depositional history of the Wyoming Province. Precambrian Research, 117(1), 119-143.

Rollinson, H.R. (2014) Using geochemical data: evaluation, presentation, interpretation. Routledge.

Ross, M., Smith, W.L., and Ashton, W.H. (1968) Triclinic talc and associated amphiboles from Gouverneur mining district New York. American Mineralogist, 53(5-6), 751-&.

Sharma, R., Joshi, P., and Pant, P. (2009) The role of fluids in the formation of talc deposits of Rema area, Kumaun Lesser Himalaya. Journal of the Geological Society of India, 73(2), 237-248.

Spandler, C., Hermann, J., Faure, K., Mavrogenes, J.A., and Arculus, R.J. (2008) The importance of talc and chlorite “hybrid” rocks for volatile recycling through subduction zones; evidence from the high-pressure subduction mélange of New Caledonia. Contributions to Mineralogy and Petrology, 155(2), 181-198.

Stemple, I.S., and Brindley, G. (1960) A Structural Study of Talc and Talc-Tremolite Relations. Journal of the American Ceramic Society, 43(1), 34-42.

Tornos, F., and Spiro, B.F. (2000) The geology and isotope geochemistry of the talc deposits of Puebla de Lillo (Cantabrian Zone, Northern Spain). Economic Geology, 95(6), 1277-1296.

Van Gosen, B.S., Lowers, H.A., Sutley, S.J., and Gent, C.A. (2004) Using the geologic setting of talc deposits as an indicator of amphibole asbestos content. Environmental Geology, 45(7), 920-939.

Virta, R.L. (1985) The phase relationship of talc and amphiboles in a fibrous talc sample. US Department of the Interior, Bureau of Mines.

Viti, C., and Collettini, C. (2009) Growth and deformation mechanisms of talc along a natural fault: a micro/nanostructural investigation. Contributions to Mineralogy and Petrology, 158(4), 529-542.